



CERN-EP-2022-070
29 March 2022

Measurement of the production of charm jets tagged with D^0 mesons in pp collisions at $\sqrt{s} = 5.02$ and 13 TeV

ALICE Collaboration*

Abstract

The measurement of the production of charm jets, identified by the presence of a D^0 meson in the jet constituents, is presented in proton–proton collisions at centre-of-mass energies of $\sqrt{s} = 5.02$ and 13 TeV with the ALICE detector at the CERN LHC. The D^0 mesons were reconstructed from their hadronic decay $D^0 \rightarrow K^- \pi^+$ and the respective charge conjugate. Jets were reconstructed from D^0 -meson candidates and charged particles using the anti- k_T algorithm, in the jet transverse momentum range $5 < p_{T,\text{chjet}} < 50$ GeV/ c , pseudorapidity $|\eta_{\text{jet}}| < 0.9 - R$, and with the jet resolution parameters $R = 0.2, 0.4, 0.6$. The distribution of the jet momentum fraction carried by a D^0 meson along the jet axis ($z_{\parallel}^{\text{ch}}$) was measured in the range $0.4 < z_{\parallel}^{\text{ch}} < 1.0$ in four ranges of the jet transverse momentum. Comparisons of results for different collision energies and jet resolution parameters are also presented. The measurements are compared to predictions from Monte Carlo event generators based on leading-order and next-to-leading-order perturbative quantum chromodynamics calculations. A generally good description of the main features of the data is obtained in spite of a few discrepancies at low $p_{T,\text{chjet}}$. Measurements were also done for $R = 0.3$ at $\sqrt{s} = 5.02$ TeV and are shown along with their comparisons to theoretical predictions in an appendix to this paper.

*See Appendix B for the list of collaboration members

1 Introduction

In high-energy proton–proton (pp) collisions, heavy quarks (charm and beauty) are produced in hard scatterings between the partons of the incoming protons. Since their masses are greater than the quantum chromodynamics (QCD) non-perturbative scale Λ_{QCD} , the production cross section of heavy quarks can be calculated using perturbative QCD (pQCD) methods [1–6]. For example, the Fixed-Order-Next-to-Leading-Logarithm (FONLL) [4] and General-Mass Variable-Flavor-Number Scheme (GM-VFNS) [5, 6] pQCD calculations can describe measurements of heavy-flavour meson production in pp collisions at RHIC and LHC energies and the $p\bar{p}$ collision data at the SPS and Tevatron [7–14].

Measurements of the production and substructure properties of heavy-flavour tagged jets provide additional information to that given by heavy-flavour hadron production. They offer a different sensitivity to study heavy-quark production processes and the contribution from higher-order processes, like gluon splitting and flavour excitation, which is useful to test pQCD calculations and tune Monte Carlo (MC) event generators [15, 16]. The transverse-momentum (p_T) differential production cross sections of charm and beauty jets were measured at the LHC in pp collisions [17–22] and were found to be consistent with next-to-leading order (NLO) pQCD calculations. Further insight into heavy-quark production can be obtained through measurements of fully reconstructed heavy-flavour hadrons inside jets and studies of the jet momentum (or energy) fraction carried by the heavy-flavour hadron, $z_{||}$, along the jet axis direction. Studies of charm jets, containing $D^{*\pm}$ mesons, were performed in pp collisions at RHIC at centre-of-mass energy $\sqrt{s} = 200$ GeV by STAR [23], CERN SPS at $\sqrt{s} = 630$ GeV by UA1 [24], LHC at $\sqrt{s} = 7$ TeV by ATLAS [20], and in $p\bar{p}$ collisions at Tevatron at $\sqrt{s} = 1.8$ TeV by CDF [25]. These measurements showed that the $z_{||}$ distribution is peaked at low $z_{||}$ values. The STAR low- $z_{||}$ enhancement cannot be described by event generators that include the leading-order charm-pair creation process ($gg/q\bar{q} \rightarrow c\bar{c}$) only. Also, the shape of the $z_{||}$ distributions measured by ATLAS is in disagreement with predictions from various Monte Carlo event generators at small values of $z_{||}$. On the other hand, the $z_{||}$ distributions at $\sqrt{s} = 7$ TeV measured by the ALICE Collaboration are in good agreement with next-to-leading order pQCD calculations and different Monte Carlo event generator predictions [18]. These observations showed the need of further model refinements and suggest the importance of the contribution of higher-order processes to charm-quark production, e.g. the ATLAS data can be described by enhancing the gluon-to-D meson fragmentation function [26]. It should be noted that ALICE and ATLAS measurements used different experimental methods and correction techniques as discussed in [18].

The heavy-flavour hadron in-jet fragmentation data can also help in constraining the gluon fragmentation functions (FFs). The FFs are usually assumed to be universal and are constrained from semi-inclusive electron–positron annihilation (SIA) data [27, 28]. The ATLAS measurement of the jet momentum fraction carried by $D^{*\pm}$ mesons [20] proved to be an important ingredient (together with SIA and the inclusive hadron production data) in the global fit analysis based on the Zero-Mass Variable-Flavor-Number Scheme (ZM-VFNS) [15]. The new ALICE results presented in this paper, from two collision energies and for lower transverse momentum ranges, provide a valuable complementary input to this global fit analysis.

Furthermore, understanding the heavy-flavour jet production in pp collisions is crucial for the interpretation of results from collisions of heavy nuclei [29]. Lattice QCD calculations [30–32] predict that in ultra-relativistic heavy-ion collisions, a state of matter known as the quark–gluon plasma (QGP), where quarks and gluons are deconfined, can be produced [33, 34]. Heavy quarks are dominantly produced in hard scatterings at the initial stage of a collision, before the QGP formation, and their thermal production in the QGP is negligible. They traverse the medium and lose part of their energy via collisional and radiative processes [35]. Therefore, heavy quarks are ideal tomographic probes [36] of the QGP [37–41], allowing extraction of the medium transport properties [42–46]. Studies of jets including heavy-flavour hadrons in such collisions can set additional constraints on the heavy-quark energy loss mechanism and the medium properties as they provide insight into how the lost energy is radiated and dissipated in the

medium.

In this paper, ALICE results on track-based jets (i.e. reconstructed using charged-particle constituents), tagged with the presence of a fully reconstructed D⁰ meson (D⁰ jet), in pp collisions at $\sqrt{s} = 5.02$ TeV and $\sqrt{s} = 13$ TeV at midrapidity are presented. Thus, the z_{\parallel} variable associated with charged tracks is better denoted as $z_{\parallel}^{\text{ch}}$. These measurements extend the previous ALICE charm jet studies in pp collisions at $\sqrt{s} = 7$ TeV [18]. The better precision obtained with these new data samples allowed more differential D⁰-jet studies to be conducted as a function of the jet resolution parameter (R) and to measure the $z_{\parallel}^{\text{ch}}$ distributions in a larger number of charged-jet transverse momentum $p_{\text{T, chjet}}$ intervals. The D⁰-jet $p_{\text{T, chjet}}$ -differential cross sections and $z_{\parallel}^{\text{ch}}$ distributions are reported in several $p_{\text{T, chjet}}$ ranges between 5 and 50 GeV/ c and for $R = 0.2, 0.4, 0.6$. The $z_{\parallel}^{\text{ch}}$ variable is defined in this article as

$$z_{\parallel}^{\text{ch}} = \frac{\vec{p}_{\text{chjet}} \cdot \vec{p}_{\text{D}^0}}{|\vec{p}_{\text{chjet}}| |\vec{p}_{\text{D}^0}|}, \quad (1)$$

where \vec{p}_{D^0} is the total D⁰-meson momentum and \vec{p}_{chjet} is the total track-based jet momentum. Ratios of the $p_{\text{T, chjet}}$ cross sections obtained for the two energies and with different R values are also presented. The R dependence is sensitive to both perturbative and non-perturbative physics of the jet production and fragmentation, and provides information on the parton shower development [47]. The results are compared to predictions of the Monte Carlo PYTHIA 8.2 [48] event generator and NLO pQCD POWHEG [49, 50] calculations, matched to the PYTHIA 8 parton shower.

This paper is organised as follows: Section 2 describes the ALICE detector and the utilised data samples, Sections 3 and 4 provide details on the analysis procedure and the systematic uncertainties, respectively. Section 5 presents the final results compared to different model predictions. Finally, conclusions are given in Section 6.

2 Detector and data sample

The reconstruction of heavy-flavour hadrons and charged jets in this analysis is done with three detectors located within a large solenoid in the central barrel of the ALICE experimental setup [51]: the Time Projection Chamber (TPC), the Inner Tracking System (ITS), and the Time-Of-Flight detector (TOF). The TPC is a gaseous drift chamber detector used for track reconstruction and particle identification (PID), thanks to the measurement of the specific energy loss of particles in the detector gas due to ionisation. The ITS, a six-layer cylindrical silicon detector, complements the track reconstruction in the TPC, allowing for a precise determination of particle trajectories in the vicinity of the collision point and the identification of charm-hadron decay vertices displaced by tens-to-hundreds of microns from the collision point. The resolution on the track impact parameter in the transverse plane to the primary vertex is better than 75 μm for tracks with $p_{\text{T}} > 1$ GeV/ c [52]. Furthermore, the effectiveness of pion/kaon separation is enhanced by the TOF, a multi-gap resistive plate chamber detector, providing the time of flight of particles from the interaction point. Due to the low magnetic field (0.5 T), ALICE is capable of reconstructing low-momentum particles down to p_{T} lower than 150 MeV/ c . The central barrel detectors cover the pseudorapidity range $|\eta| < 0.9$ and full azimuthal angle of $\varphi \in [0, 2\pi]$. To provide uniform pseudorapidity acceptance, only those events having a primary vertex within ± 10 cm from the nominal beam collision position along the beam direction were analysed.

Events with the least possible bias were selected using a minimum bias trigger which helped in identifying beam–beam collisions by requiring an event to be accepted only if a signal was found in both scintillator arrays of the V0 detector covering the pseudorapidity intervals $-3.7 < \eta < -1.7$ and $2.8 < \eta < 5.1$. The V0 detector was used in combination with the Silicon Pixel Detector (SPD), which comprises the first two layers of the ITS, to reduce the background due to beam–gas interactions. In addition, a dedi-

cated algorithm based on multiple-vertex searches in the SPD was used in order to reduce pile-up events containing two or more primary vertices.

The data samples analysed in this paper consist of 0.99×10^9 minimum bias events from pp collisions at $\sqrt{s} = 5.02$ TeV recorded in 2017, corresponding to an integrated luminosity of $\mathcal{L}_{int} = (19.3 \pm 0.4) \text{ nb}^{-1}$ [53], and 1.49×10^9 minimum bias events taken at $\sqrt{s} = 13$ TeV between 2016 and 2018, corresponding to an integrated luminosity of $\mathcal{L}_{int} = (25.81 \pm 0.43) \text{ nb}^{-1}$ [54].

The Monte Carlo samples used for the corrections, described in Section 3.3, were produced with the PYTHIA 6.4.25 event generator [55], with the Perugia 2011 tune [56] and the GEANT 3.21.11 [57] transport model. The ALICE detector layout and the variations of the data-taking conditions during the run were reproduced in the simulation. They shall be referred to as PYTHIA 6 and GEANT 3 in the following, unless otherwise specified. The reconstruction procedure of jets containing D⁰ mesons is briefly illustrated in the following section.

3 D⁰ meson tagged jet reconstruction and corrections

3.1 D⁰ meson and jet reconstruction

The D⁰ mesons were reconstructed via their hadronic decay channel $D^0 \rightarrow K^- \pi^+$ and its charge conjugate ($\text{BR} = 3.950 \pm 0.031\%$) [58]. The D⁰ meson and its anti-particle are treated equivalently and shall both be referred to as D⁰ in the following, unless otherwise specified. The D⁰ mesons produced directly in the charm-quark fragmentation or in decays of directly-produced excited charm hadron states are called prompt D⁰ mesons, and those that originate from decays of beauty hadrons are denoted as non-prompt D⁰ mesons.

The D⁰ candidates were constructed by combining oppositely charged tracks identified as π or K mesons. These tracks were required to have $p_T > 300 \text{ MeV}/c$, $|\eta| < 0.8$, a minimum of 70 crossed rows in the TPC, with at least 80% of these having an associated cluster of charged signals in the TPC end plates, and at least two hits in the ITS, with a minimum of one of these in the two innermost layers. For tracks with $p_T < 3 \text{ GeV}/c$, a hit in the innermost layer of the ITS was also required. With the mentioned kinematic selections on the pion and kaon tracks, the D⁰-meson acceptance in rapidity is p_{T,D^0} -dependent with the upper limit growing from $|y_D| = 0.5$ at $p_{T,D^0} = 0$ to $|y_D| = 0.8$ at $p_{T,D^0} = 5 \text{ GeV}/c$. The particle identification was carried out by exploiting the specific energy loss dE/dx in the TPC and the time-of-flight provided by the TOF detector. Pions and kaons were selected within 3σ (with σ being the resolution on the dE/dx and the time-of-flight) from the expected mean values. Particles with no TOF information were identified using the TPC information only. In order to reduce the combinatorial background, geometrical selections on the D⁰-decay topology were applied, exploiting the displacement (typically of a few hundred μm) of the D⁰-meson decay vertices from the primary vertex of the interaction. The selection was tuned to provide a high D⁰ signal-to-background ratio. Further details about the track and D⁰-candidate selections can be found in Ref. [59–61].

For the jet reconstruction, charged particles were used and were required to have $p_T > 150 \text{ MeV}/c$ and $|\eta| < 0.9$. The track selection criteria applied were less stringent than those applied to the D⁰-daughter tracks in order to ensure a flat acceptance in η and ϕ . Jets were reconstructed with the anti- k_T clustering algorithm as implemented in the FastJet package [62] with the resolution parameters $R = 0.2, 0.4, 0.6$, using the p_T recombination scheme. To ensure that the whole jet was contained within the detector acceptance, jets were required to have their axes within the pseudorapidity range of $|\eta_{jet}| < 0.9 - R$. At low momenta, D⁰-decay products can be emitted at angles larger than the defined jet cone size. In order to ensure that the π and K mesons from the D⁰ decay were assigned to the same jet, they were removed from the set of charged-particle tracks before the jet reconstruction and their four-momenta were replaced by that of the D⁰ candidate. A charm jet was tagged by the presence of a D⁰-meson candidate among its

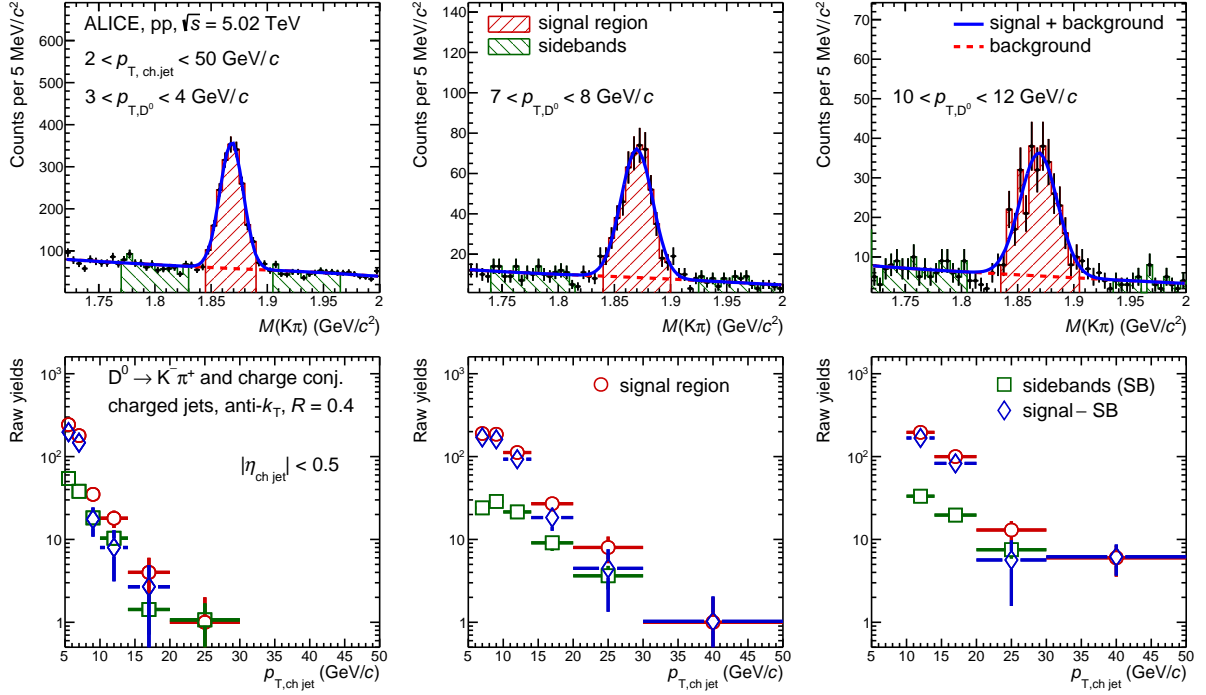


Figure 1: Top: invariant mass distributions of D⁰-jet candidates for $2 < p_{T,\text{ch,jet}} < 50$ GeV/ c and $R = 0.4$ in pp collisions at $\sqrt{s} = 5.02$ TeV, in the D⁰-meson transverse momentum intervals: $3 < p_{T,D^0} < 4$ GeV/ c (left), $7 < p_{T,D^0} < 8$ GeV/ c (centre), and $10 < p_{T,D^0} < 12$ GeV/ c (right). The total fit function is represented by the blue solid line, while the red dashed line represents the sum of the background and reflection fit functions. The red and green shaded areas correspond to the peak and sideband regions, respectively. Bottom: D⁰-jet raw yields as a function of $p_{T,\text{ch,jet}}$ in the signal and sideband regions, and their subtracted yields.

constituents. In the rare case in which more than one D⁰-meson candidate was present, the procedure was repeated separately for each D⁰-meson candidate in the event. No correction for the background coming from the underlying event was applied. The analysis procedure closely followed previous ALICE studies of charm jets tagged with D⁰ mesons [18].

3.2 Raw yield extraction

Raw yields of D⁰ jets were obtained using a statistical approach. Oppositely charged kaons and pions from the decays of the D⁰-meson candidates were combined and the pair's invariant mass distribution (M) was extracted in several intervals of D⁰-meson transverse momentum within $2 < p_{T,D^0} < 36$ GeV/ c . For the $z_{\parallel}^{\text{ch}}$ studies, the D⁰-jet signal was also split in different ranges of $p_{T,\text{ch,jet}}$. The M distributions were fitted with a function composed of a Gaussian for the D⁰-signal peak and an exponential for the background. When two oppositely charged pion and kaon tracks are combined to form a D⁰ candidate, it may happen that neither the kaon nor the pion hypothesis can be definitively excluded for either of the tracks. In that case, the pair was accepted both as a D⁰ and a \bar{D}^0 candidate, and the two related invariant mass values, resulting from swapping the pion and kaon mass hypotheses for the two tracks, were considered in the analysis. The candidates corresponding to a real D⁰ (or \bar{D}^0) meson but with the wrong decay-product mass assignment are referred to as reflections. The reflection component was included in the invariant mass fitting procedure and subtracted from the signal. The reflection templates were obtained from simulations with the PYTHIA 6 event generator and parametrised as a sum of two Gaussians with the means, widths, and the D⁰ signal-over-reflection ratio fixed to values obtained in the simulations.

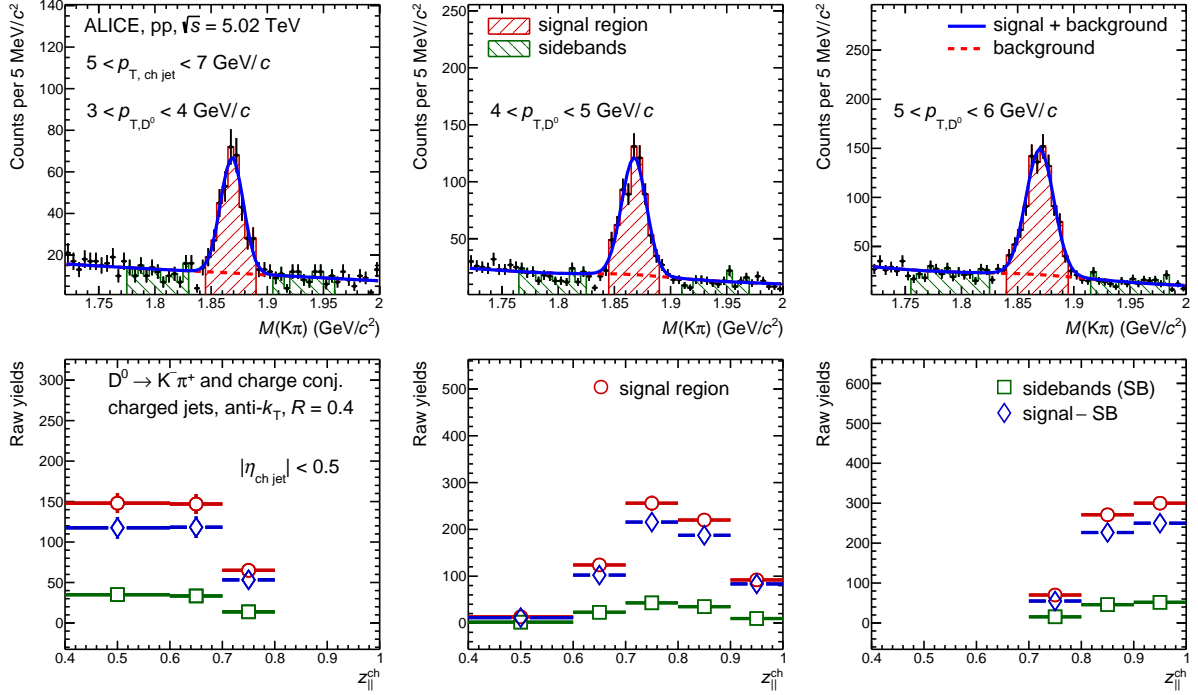


Figure 2: Top: invariant mass distribution of D⁰-jet candidates for one jet- p_T interval of $5 < p_{T,\text{chjet}} < 7$ GeV/ c and $R = 0.4$ in pp collisions at $\sqrt{s} = 5.02$ TeV, in D⁰-meson transverse momentum intervals: $3 < p_{T,D^0} < 4$ GeV/ c (left), $4 < p_{T,D^0} < 5$ GeV/ c (centre), and $5 < p_{T,D^0} < 6$ GeV/ c (right). The total fit function is represented by the blue solid line, while the red dashed line represents the background fit function. The red and green shaded areas correspond to the peak and sideband regions, respectively. Bottom: D⁰-jet raw yields as a function of $z_{\parallel}^{\text{ch}}$ in the signal and sideband regions, and their subtracted yields.

The signal region was defined to be within $|M - \mu_{\text{fit}}| < 2\sigma_{\text{fit}}$, where μ_{fit} is the mean and σ_{fit} is the width of the Gaussian fit component, respectively. The background regions (sidebands) were chosen as follows: $4\sigma_{\text{fit}} < |M - \mu_{\text{fit}}| < 9\sigma_{\text{fit}}$. The top panels of Fig. 1 and 2 show examples of M distributions for different intervals of p_{T,D^0} . The signal and sideband regions are represented by the dashed red and green areas, respectively. The reflection contributions are included in the background fit function. The bottom panels of Fig. 1 and 2 present the raw yields of D⁰ jets as a function of $p_{T,\text{chjet}}$ and $z_{\parallel}^{\text{ch}}$ extracted for the signal and sideband M regions in each p_{T,D^0} interval. The sideband distributions were normalised to the background yield in the peak region and subtracted from the signal-region distributions in order to obtain the raw D⁰-jet $p_{T,\text{chjet}}$ and $z_{\parallel}^{\text{ch}}$ distributions.

3.3 Corrections

A threefold correction was applied to the raw D⁰-jet $p_{T,\text{chjet}}$ and $z_{\parallel}^{\text{ch}}$ distributions. The corrections account for: (i) the efficiency and acceptance of the D⁰-jet reconstruction, (ii) the contribution of D⁰ mesons originating from b-hadron decays, and (iii) the momentum smearing introduced by detector effects. The systematic uncertainties of these corrections are discussed in Sec. 4.

3.3.1 Reconstruction efficiency

The reconstruction efficiency of the D⁰ jets within the detector acceptance was calculated using the simulation described in Section 2. The efficiency was defined as the ratio of D⁰ jets that passed all the data analysis selection requirements to all generated D⁰ jets within $|\eta_{\text{jet}}| < 0.9 - R$. The efficiency depends on the D⁰-meson topological selections, which are stricter at low p_{T,D^0} in order to reduce the

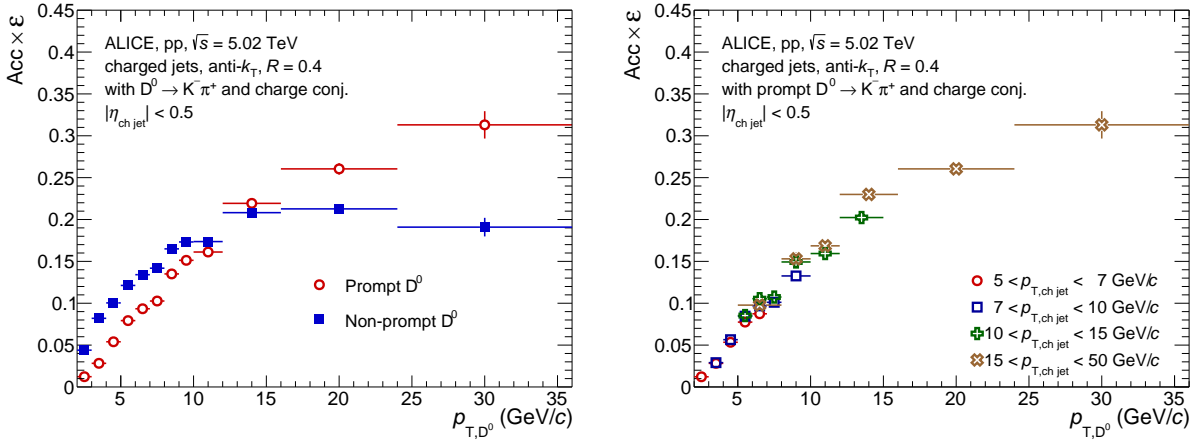


Figure 3: Product of acceptance and efficiency, $\text{Acc} \times \epsilon$, for D⁰-jet reconstruction as a function of p_{T,D^0} with $R = 0.4$ in pp collisions at $\sqrt{s} = 5.02$ TeV. Left: $\text{Acc} \times \epsilon$ for prompt and non-prompt D⁰ jets in the range $5 < p_{T,\text{ch,jet}} < 50$ GeV/c. Right: $\text{Acc} \times \epsilon$ for prompt D⁰ jets in different jet- p_T intervals.

larger combinatorial background present in this kinematic region. Therefore, the D⁰-jet reconstruction efficiency depends strongly on p_{T,D^0} , but has negligible dependence on $p_{T,\text{ch,jet}}$ in the measured ranges. Fig. 3 (left) shows the product of acceptance and efficiency for prompt and non-prompt D⁰ jets. The acceptance and efficiency for non-prompt D⁰ jets tends to be higher than that for prompt D⁰ jets at low p_{T,D^0} with a crossing point around $p_{T,D^0} = 15$ GeV/c. The non-prompt D⁰ mesons are selected with higher efficiency because of their larger displacement from the primary vertex. However, at higher p_{T,D^0} , a selection on the impact parameters of the decay particles suppresses the non-prompt contribution while keeping most of the prompt ones. Both efficiencies are independent of the $p_{T,\text{ch,jet}}$ selection as is seen for the prompt efficiencies in different analysed $p_{T,\text{ch,jet}}$ intervals in Fig. 3 (right).

The product of the acceptance (Acc) and the reconstruction efficiency (ϵ) of the prompt D⁰ jets was used to correct the raw yields extracted in different intervals of p_{T,D^0} , as described in Section 3.2. The efficiency-corrected $p_{T,\text{ch,jet}}$ distributions were then summed over all the p_{T,D^0} intervals, according to

$$N(p_{T,\text{ch,jet}}) = \sum_{p_{T,D^0}} \frac{N_{\text{raw}}(p_{T,\text{ch,jet}}, p_{T,D^0})}{(\text{Acc} \times \epsilon)_c(p_{T,D^0})}, \quad (2)$$

where c represents charm (prompt D⁰ mesons) and N is the total efficiency-corrected yield. A similar method was also used to extract efficiency-corrected $z_{\parallel}^{\text{ch}}$ distributions in different p_{T,D^0} and $p_{T,\text{ch,jet}}$ intervals.

3.3.2 Subtraction of b-jet contribution

Since the natural fraction of D⁰ mesons originating from b-quark fragmentation is biased by the applied topological selection criteria, the non-prompt D⁰-meson contribution was subtracted from the reported distributions to get the desired prompt D⁰-jet distributions (N^c). The limited sample size did not allow for a data-driven estimation of the non-prompt D⁰-jet fraction. Therefore, NLO pQCD calculations of POWHEG [49, 50, 63, 64] coupled to the PYTHIA 6 [55, 56] MC parton shower were used to estimate this contribution. There are three parameters in the calculations: the beauty-quark mass (m_b) that was set to $m_b = 4.75$ GeV/ c^2 , and the renormalisation (μ_R) and factorisation (μ_F) scales, both set to the quark transverse mass $\mu_R = \mu_F = \sqrt{m_b^2 + p_T^2}$. Parton distribution functions (PDF) obtained from the CT10NLO set [65] using the LHAPDF6 [66] interpolator were used.

The simulation output was scaled by the ratio of the reconstruction efficiencies of non-prompt and prompt

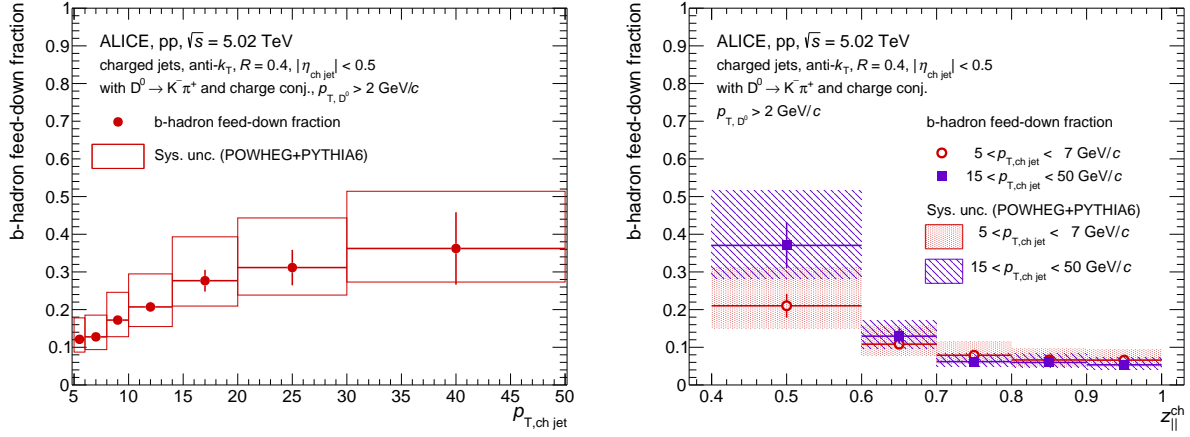


Figure 4: Feed-down fraction of D⁰ jets from b-hadrons in pp collisions at $\sqrt{s} = 5.02$ TeV for $R = 0.4$ as a function of $p_{T,\text{chjet}}$ in $5 < p_{T,\text{chjet}} < 50$ GeV/c (left) and as a function of $z_{\parallel}^{\text{ch}}$ in two $p_{T,\text{chjet}}$ intervals $5 < p_{T,\text{chjet}} < 7$ GeV/c and $15 < p_{T,\text{chjet}} < 50$ GeV/c (right).

D⁰ jets ($\varepsilon_b/\varepsilon_c$) because ε_b -scaled non-prompt simulations ($\varepsilon_b \times N_{\text{POWHEG}}^b$) are comparable with ε_c -scaled prompt D⁰-jet distributions ($\varepsilon_c \times N^c$). In the next step, the POWHEG + PYTHIA 6 $p_{T,\text{chjet}}$ ($z_{\parallel}^{\text{ch}}$) distributions were smeared using a response matrix (RM) for non-prompt D⁰ jets, $\text{RM}_{b \rightarrow D^0}$, which maps the D⁰-jet particle-level variables ($p_{T,\text{chjet}}^{\text{part}}, z_{\parallel}^{\text{ch,part}}$) from PYTHIA 6 simulations to the detector-level variables ($p_{T,\text{chjet}}^{\text{det}}, z_{\parallel}^{\text{ch,det}}$) reconstructed in full PYTHIA 6 + GEANT 3 detector simulations. The RM was also re-weighted by the prompt D⁰-jet efficiency to address the fact that the measured sample is already corrected by it. A correction was made to account for jets which were inside the detector acceptance but outside the generated range, and for those which were outside of the acceptance but inside the generated range. The calculated b-jet feed-down fraction in the measured sample is shown in Fig. 4 as a function of $p_{T,\text{chjet}}$ and $z_{\parallel}^{\text{ch}}$. The estimation of the corresponding systematic uncertainties shown in Fig. 4 is described in Section 4.

The b-hadron feed-down contribution was then subtracted from the efficiency-corrected $p_{T,\text{chjet}}$ distributions according to

$$N^c(p_{T,\text{chjet}}^{\text{det}}) = N(p_{T,\text{chjet}}^{\text{det}}) - \sum_{p_{T,D^0}} \text{RM}_{b \rightarrow D^0}(p_{T,\text{chjet}}^{\text{det}}, p_{T,\text{chjet}}^{\text{part}}, p_{T,D^0}) \otimes \sum_{p_{T,D^0}} \frac{(\text{Acc} \times \varepsilon)_b(p_{T,D^0})}{(\text{Acc} \times \varepsilon)_c(p_{T,D^0})} N_{\text{POWHEG}}^b(p_{T,D^0}, p_{T,\text{chjet}}^{\text{part}}), \quad (3)$$

where:

- c and b stand for charm (prompt D⁰) and beauty (non-prompt D⁰), respectively;
- $N(p_{T,\text{chjet}}^{\text{det}})$ is the total efficiency-corrected measured yield, before subtraction of the b-jet contribution;
- $N^c(p_{T,\text{chjet}}^{\text{det}})$ is the efficiency-corrected measured yield after subtraction of the b-jet contribution;
- the symbol \otimes should be interpreted as the convolution of the non-prompt $\text{RM}_{b \rightarrow D^0}$ and the vector of the yields;

- $(\text{Acc} \times \varepsilon)_c(p_{T,D^0})$, $(\text{Acc} \times \varepsilon)_b(p_{T,D^0})$ are the p_{T,D^0} -dependent products of the acceptance and the reconstruction efficiency for prompt and non-prompt D⁰ jets respectively;
- $N_{\text{POWHEG}}^b(p_{T,D^0}, p_{T,\text{chjet}}^{\text{part}})$ is the non-prompt D⁰-jet $p_{T,\text{chjet}}$ cross section from the POWHEG simulation scaled by the integrated luminosity of the analysed data.

An analogous subtraction was also performed for the $z_{\parallel}^{\text{ch}}$ studies.

3.3.3 Unfolding

The measured $p_{T,\text{chjet}}$ and $z_{\parallel}^{\text{ch}}$ distributions were corrected for the detector resolution and track momentum smearing. The corrections were encoded in a detector RM that mapped the D⁰-jet particle-level variables ($p_{T,\text{chjet}}^{\text{part}}, z_{\parallel}^{\text{ch,part}}$) from PYTHIA 6 simulations to the detector-level variables ($p_{T,\text{chjet}}^{\text{det}}, z_{\parallel}^{\text{ch,det}}$) reconstructed in full PYTHIA 6 + GEANT 3 detector simulations. The detector and particle-level charged-particle jets were matched by requiring the same prompt D⁰ meson among their constituents. The jets at both levels were reconstructed using the anti- k_T clustering algorithm. The 1-dimensional RM used to correct for the $p_{T,\text{chjet}}$ and the corresponding relative resolution, defined as $\Delta_p = (p_{T,\text{chjet}}^{\text{det}} - p_{T,\text{chjet}}^{\text{part}})/p_{T,\text{chjet}}^{\text{part}}$, are displayed in Fig. 5. Fig. 6 presents the 2-dimensional RM for the $z_{\parallel}^{\text{ch}}$ and $p_{T,\text{chjet}}$ variables, along with the relative resolution $\Delta_z = (z_{\parallel}^{\text{ch,det}} - z_{\parallel}^{\text{ch,part}})/z_{\parallel}^{\text{ch,part}}$ for a given $p_{T,\text{chjet}}$ interval.

The finite detector resolution modifies the measured yields as a function of $p_{T,\text{chjet}}$ and $z_{\parallel}^{\text{ch}}$. They were therefore unfolded using an iterative method based on Bayes' theorem [67] as implemented in the RooUnfold package [68]. The $p_{T,\text{chjet}}$ spectra were unfolded using a 1D unfolding method, while for the $z_{\parallel}^{\text{ch}}$ distributions a 2D method was implemented. The RM was scaled by the prompt D⁰-jet efficiency before unfolding the measured spectra. Five iterations showed to be optimal, representing a good convergence of the unfolding, and were chosen as the default. The unfolding was performed in the following ranges: $2 < p_{T,\text{chjet}} < 50$ GeV/ c and $0.4 < z_{\parallel}^{\text{ch}} < 1$. Similar to the correction of non-prompt D⁰-jet simulations, the measured spectra were also corrected for in order to account for jets which were inside the detector acceptance but outside the generated range, and for those which were outside of the acceptance but inside the generated range. This resulted in a correction of about 1–2%.

To verify the stability of the unfolding and the choice of the number of iterations, several checks were performed. Firstly, the unfolded spectra were folded back and compared to the original data. A good agreement was found in all the cases. Secondly, Pearson correlation coefficients were calculated to determine the optimal number of iterations and lastly, a closure test was performed which also provided an estimate of the systematic uncertainty of the method and is described in more detail in Section 4. While the reported range is $5 < p_{T,\text{chjet}} < 50$ GeV/ c , the measurements in the $2 < p_{T,\text{chjet}} < 5$ GeV/ c interval were kept in the unfolding for both $p_{T,\text{chjet}}$ and $z_{\parallel}^{\text{ch}}$ to avoid potential biases due to edge effects.

4 Systematic uncertainties

Several sources of systematic uncertainties were studied and can be separated into the following groups: (i) D⁰-meson selections, (ii) raw yield extraction, (iii) beauty feed-down, (iv) unfolding, (v) track-reconstruction efficiency, and (vi) normalisation.

Discrepancies between data and simulations for the distributions of variables used in the D⁰-meson selections can impact on the D⁰-jet reconstruction efficiency. In order to assign a systematic uncertainty from this source, the D⁰-meson topological selections were varied and the whole analysis procedure was repeated for each variation. The test spanned a variation of the reconstruction efficiency between 10% and 25%, depending on the D⁰-meson p_T . The uncertainty was estimated by taking the root-mean-square of the results obtained with the different D⁰-meson selection criteria. The uncertainty increases with $p_{T,\text{chjet}}$

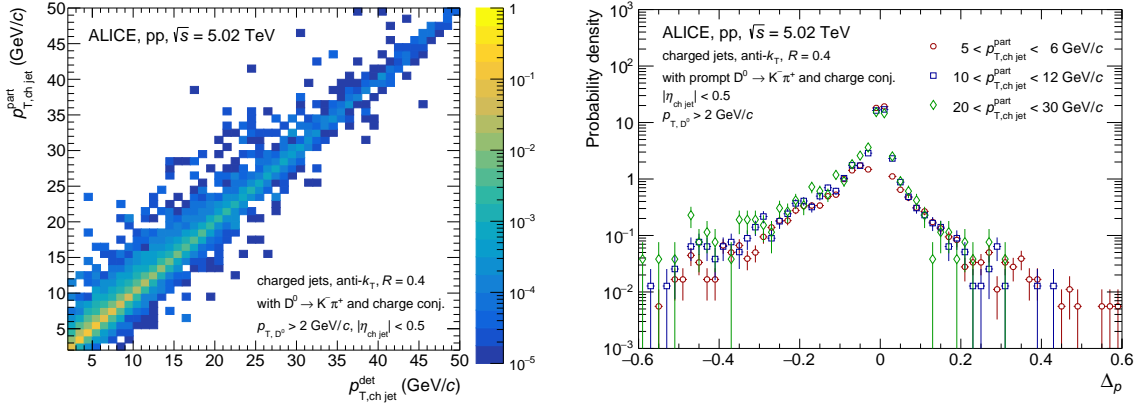


Figure 5: Left: detector response matrix of matched jets used for unfolding the $p_{T,\text{chjet}}$ distribution with $R = 0.4$ in pp collisions at $\sqrt{s} = 5.02$ TeV in the range $2 < p_{T,\text{chjet}} < 50$ GeV/c. Right: $p_{T,\text{chjet}}$ resolution, Δ_p , for $5 < p_{T,\text{chjet}}^{\text{part}} < 6$ GeV/c, $10 < p_{T,\text{chjet}}^{\text{part}} < 12$ GeV/c, and $20 < p_{T,\text{chjet}}^{\text{part}} < 30$ GeV/c.

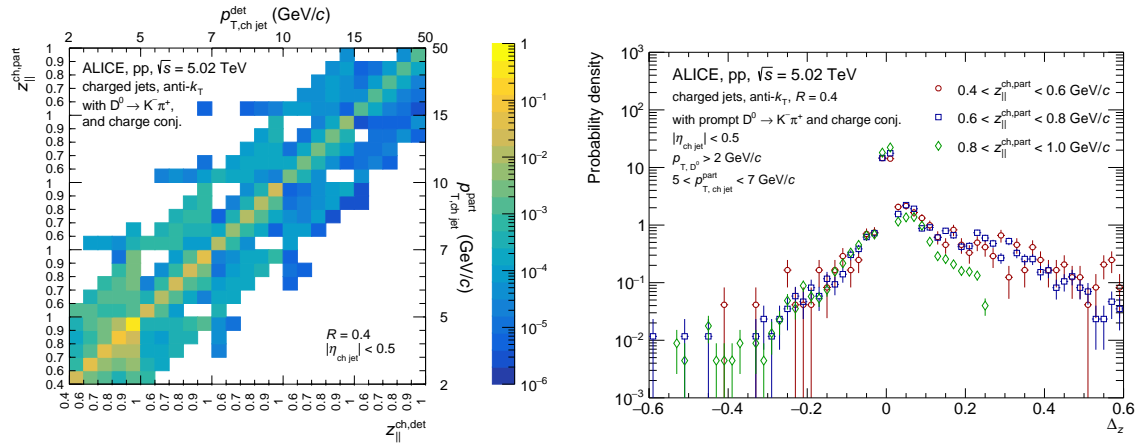


Figure 6: Left: detector response matrix of matched jets used for unfolding $z_{||}^{\text{ch}}$ distribution with $R = 0.4$ in pp collisions at $\sqrt{s} = 5.02$ TeV in the range $2 < p_{T,\text{chjet}} < 50$ GeV/c and $0.4 < z_{||}^{\text{ch}} < 1$. Right: $z_{||}^{\text{ch}}$ resolution, Δ_z , in the $z_{||}^{\text{ch,part}}$ intervals 0.4–0.6, 0.6–0.8, and 0.8–1 for the $p_{T,\text{chjet}}$ interval $5 < p_{T,\text{chjet}}^{\text{part}} < 7$ GeV/c.

and decreases with $z_{||}^{\text{ch}}$, and varies between 1% and 10% for the sample at $\sqrt{s} = 13$ TeV and between 3% and 25% for $\sqrt{s} = 5.02$ TeV. The particle identification related systematic uncertainties for D⁰-meson selections were negligible [59] and excluded from the calculation.

The stability of the raw yield extraction procedure described in Section 3.2 was assessed by performing multiple trials of the invariant mass fit while varying the fitting conditions. The conditions that were varied are: (i) the assumed shape of the background function (default exponential was replaced by linear and polynomial functions), (ii) the fit ranges, and (iii) the width (σ_{fit}) and (iv) mean (μ_{fit}) of the Gaussian signal, which were left as free parameters or fixed to the MC values. The yields obtained from the multiple trials were compared to the default one and the root-mean-square of the relative differences was taken as a part of the systematic uncertainties from the raw yield extraction. Secondly, the signal range was varied between 2 to 3 standard deviations of the signal peak width, while the sideband extraction range $|M - \mu_{\text{fit}}|$ was varied through 4–9, 4–8, 3.5–9, 3.5–8, 4.5–9, and 4.5–8 units of standard deviation. The corresponding uncertainties amount to about 1% and 2%, respectively. A third contribution to the systematic uncertainty on the raw yield extraction was assigned by varying the relative contribution of reflections by $\pm 50\%$ and the maximum deviation in the raw yield was taken as a systematic uncertainty.

The total uncertainty on the raw yield extraction was estimated to be 2–9% for the $p_{T,\text{chjet}}$ -differential cross section and 2–6% for the $z_{\parallel}^{\text{ch}}$ distributions for the $\sqrt{s} = 13$ TeV analysis. For the $\sqrt{s} = 5.02$ TeV analysis, the uncertainties reach a maximum of about 13% for the $p_{T,\text{chjet}}$ -differential cross section, and are within 8% for the $z_{\parallel}^{\text{ch}}$ distributions.

The systematic uncertainty from the subtraction of the b-hadron decay contribution was determined by varying the parameters of the non-prompt D⁰-jet POWHEG + PYTHIA 6 simulations. They were varied individually in the following ways: (i) the beauty-quark mass was changed to 4.5 GeV/ c^2 and 5 GeV/ c^2 from the default 4.75 GeV/ c^2 and (ii) μ_R and μ_F were either halved or doubled from their nominal values, which were defined as the transverse mass of the beauty quark. The largest upward and downward variations of the resulting cross sections were taken as the systematic uncertainties. The uncertainty on the prompt cross section due to the feed-down subtraction was estimated for the $p_{T,\text{chjet}}$ -differential cross section to be 5–30% for the sample at $\sqrt{s} = 13$ TeV and 4–40% for $\sqrt{s} = 5.02$ TeV. For the $z_{\parallel}^{\text{ch}}$ distributions it was 2–20% and 2–15% for $\sqrt{s} = 13$ TeV and $\sqrt{s} = 5.02$ TeV, respectively.

The systematic uncertainty on the unfolding procedure was assigned based on a MC closure test. The MC sample was randomly split into two subsamples and one part was used to build the RM while the other one was used as a test sample. The efficiency correction was applied on the test sample following the method used in the data analysis. The same unfolding procedure was then applied as in the data analysis, and the resulting distributions were compared to the generator-level MC distributions. The random split was performed ten times and a mean value of the deviations from these trials was taken as the final uncertainty of the unfolding procedure. The resulting uncertainty is 1–5% in most cases while rising with increasing $p_{T,\text{chjet}}$ and falling with increasing $z_{\parallel}^{\text{ch}}$. Occasionally, the uncertainty goes above 10% for the highest $p_{T,\text{chjet}}$ interval in $p_{T,\text{chjet}}$ distributions and for lowest $z_{\parallel}^{\text{ch}}$ intervals in $z_{\parallel}^{\text{ch}}$ distributions. In addition, several checks were performed in order to test the stability of the unfolding procedure explained in Section 3.3.3, and were treated as a procedure cross-check: (i) the default number of five iterations of the Bayesian unfolding was varied by ± 1 , (ii) the default MC generator-level prior distribution shape was varied by using the measured $p_{T,\text{chjet}}$ distribution or different parametrised power-law functions, $f(p_{T,\text{chjet}}) = p_{T,\text{chjet}}^{-a} e^{-ab/p_{T,\text{chjet}}}$ with $3 < a, b < 5$, and (iii) the true and measured ranges for $p_{T,\text{chjet}}$ spectra provided to the unfolding procedure were varied. All these tests gave consistent unfolding results with maximum relative deviations of 1%.

The measurement is also affected by uncertainties on the efficiency of the track reconstruction that influence the jet momentum resolution and the D⁰-meson reconstruction efficiency. The relative uncertainty on the reconstruction efficiency for a single track used for the jet reconstruction was estimated to be 4%. To assess the systematic uncertainty on the prompt cross section due to this source, a new detector RM was built where 4% of all the reconstructed charged tracks in the detector simulations were randomly rejected. The $p_{T,\text{chjet}}$ and $z_{\parallel}^{\text{ch}}$ distributions were then unfolded using this modified RM and the results were compared to the final distributions unfolded with the default detector RM. The relative uncertainty from this source was found to increase with $p_{T,\text{chjet}}$ reaching a maximum of 10%. The uncertainties originating from the track momentum resolution were previously studied and found to be negligible [52, 69]. For the reconstruction efficiency of D⁰-mesons, a p_{T,D^0} -independent systematic uncertainty of 5% was assigned based on the D⁰-meson studies reported in Ref. [59]. Since the reported $z_{\parallel}^{\text{ch}}$ distributions are self-normalised, this uncertainty is negligible in this case.

Finally, the normalisation of the $p_{T,\text{chjet}}$ -differential cross section was affected by a 0.8% uncertainty on the D⁰-meson decay branching ratio and by the uncertainty on the luminosity determination which is 2.1% and 1.7% for $\sqrt{s} = 5.02$ TeV and $\sqrt{s} = 13$ TeV, respectively.

The relative systematic uncertainties for D⁰ jets on their $p_{T,\text{chjet}}$ -differential cross sections for $R = 0.4$ are summarised in Table 1. The $z_{\parallel}^{\text{ch}}$ systematic uncertainties in two of the four $p_{T,\text{chjet}}$ intervals are presented in Table 2.

Table 1: Relative (%) systematic uncertainties for selected $p_{T,\text{chjet}}$ intervals of $R = 0.4$ jets at $\sqrt{s} = 5.02$ TeV and $\sqrt{s} = 13$ TeV.

$p_{T,\text{chjet}}$ (GeV/c)	\sqrt{s} (TeV)			\sqrt{s} (TeV)		
	5–6	8–10	30–50	5–6	8–10	30–50
Topological selection	3.4	5.6	25	3.6	2.9	8.8
Raw yield extraction	3.1	3.1	11	3.3	2.5	8.8
B Feed-down	+ 3.9	+ 5.3	+ 14	+ 4.7	+ 5.9	+ 12
	– 6.5	– 8.9	– 24	– 6.5	– 8.5	– 22
Unfolding	2.8	0.6	12	2.7	0.7	0.9
Tracking eff. (jet energy scale)	1.6	2.4	9.6	0.8	2.1	9.7
Tracking eff. (D-meson)	5.0	5.0	5.0	5.0	5.0	5.0
BR	0.8	0.8	0.8	0.8	0.8	0.8
Luminosity	2.1	2.1	2.1	1.7	1.7	1.7
Total	+ 9.0	+ 10	+ 35	+ 10	+ 10	+ 21
	– 10	– 13	– 40	– 11	– 12	– 28

Table 2: Relative (%) systematic uncertainties for selected $z_{\parallel}^{\text{ch}}$ and $p_{T,\text{chjet}}$ intervals of $R = 0.4$ jets at $\sqrt{s} = 5.02$ TeV and $\sqrt{s} = 13$ TeV.

$p_{T,\text{chjet}}$ (GeV/c)	\sqrt{s} (TeV)				\sqrt{s} (TeV)			
	5.02		5.02		13		13	
	5–7	7–10	5–7	7–10	5–7	7–10	5–7	7–10
$z_{\parallel}^{\text{ch}}$	0.6–0.7	0.9–1.0	0.6–0.7	0.9–1.0	0.6–0.7	0.9–1.0	0.6–0.7	0.9–1.0
Topological selection	3.8	2.3	9.2	1.4	2.8	1.7	3.6	1.1
Raw yield extraction	3.3	4.3	4.2	2.4	3.5	4.3	5.8	2.4
B Feed-down	+ 3.0	+ 1.9	+ 2.5	+ 1.2	+ 3.4	+ 2.8	+ 3.4	+ 2.2
	– 5.1	– 3.2	– 4.2	– 2.8	– 4.8	– 3.8	– 4.9	– 3.3
Unfolding	0.4	1.3	0.7	0.0	0.7	0.2	1.6	1.4
Tracking eff. (jet energy scale)	1.3	1.7	5.3	3.1	3.2	4.9	3.2	4.9
Total	+ 6.0	+ 5.6	+ 12	+ 4.5	+ 6.6	+ 7.3	+ 8.4	+ 6.1
	– 7.3	– 6.2	– 12	– 5.0	– 7.4	– 7.8	– 9.1	– 6.6

The total systematic uncertainties for the D⁰-jet $p_{T,\text{chjet}}$ -differential cross sections and the $z_{\parallel}^{\text{ch}}$ distributions were obtained by summing in quadrature the uncertainties estimated for each of the sources. In the case of cross section ratios for different jet resolution parameters, the systematic uncertainties due to tracking efficiency of the D⁰-meson decay products and the normalisation uncertainties are assumed to be fully correlated and, hence, cancel out in the ratios. Systematic uncertainties due to the D⁰-meson topological selection are partially correlated and an average of the uncertainties for two resolution parameters R was taken. Partial correlation was also assumed for the tracking efficiency related to the jet energy scale. A simultaneous-variation method was used to determine the uncertainty, i.e. the detector response matrices for two given R values were varied simultaneously and the relative uncertainty on the cross section ratio was determined by the difference of the final ratio results obtained with modified and nominal response matrices. Systematic uncertainties on the ratio of cross sections for the two colliding energies were obtained by adding them in quadrature, except for the BR uncertainty which was treated as fully correlated. No other correlation was considered given that the data taking periods and the detector conditions were different.

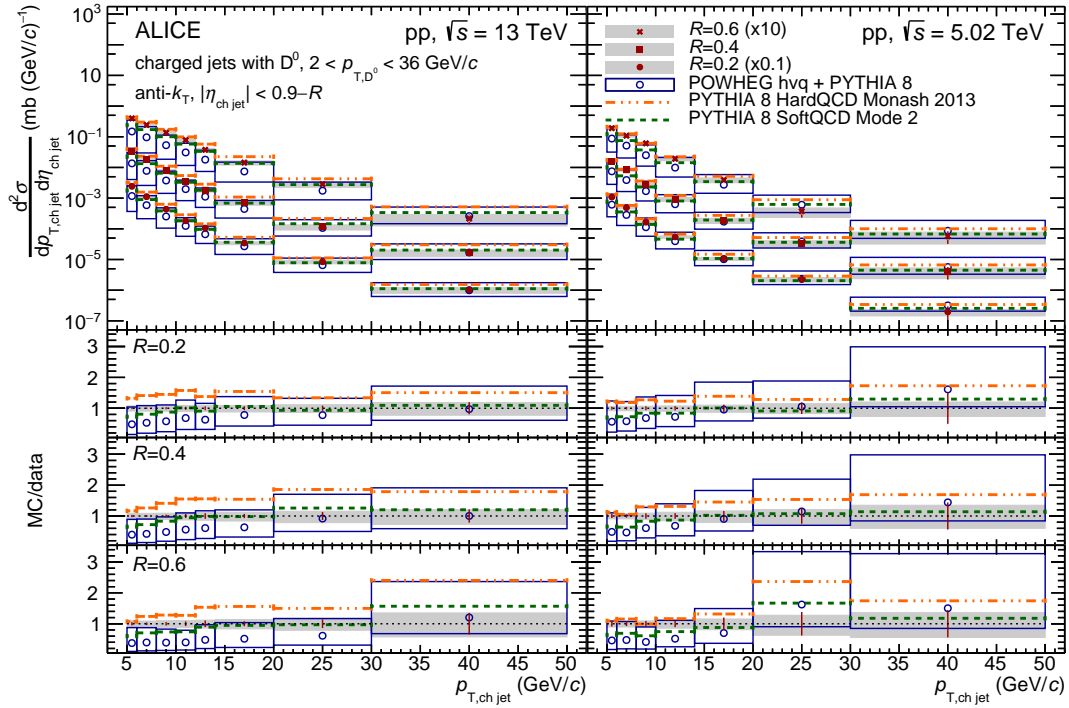


Figure 7: Top panels: $p_{T, \text{chjet}}$ -differential cross section of charm jets tagged with D^0 mesons for $R = 0.2$ (circles, scaled by 0.1), 0.4 (squares) and 0.6 (crosses, scaled by 10) in pp collisions at $\sqrt{s} = 13$ TeV (left) and $\sqrt{s} = 5.02$ TeV (right) compared to PYTHIA 8 HardQCD Monash 2013 (dash-dotted lines), PYTHIA 8 SoftQCD Mode 2 (dashed lines), and POWHEG hvq + PYTHIA 8 (open circles) predictions. The shaded bands indicate the systematic uncertainty on the data cross section while open boxes represent the theoretical uncertainties on the POWHEG predictions. Bottom panels: ratios of MC predictions to the data for $R = 0.2, 0.4$ and 0.6 .

5 Results

5.1 Transverse-momentum differential cross sections

The $p_{T, \text{chjet}}$ -differential cross section of D^0 jets is defined as

$$\frac{d^2\sigma}{dp_{T, \text{chjet}}d\eta_{\text{jet}}}(p_{T, \text{chjet}}) = \frac{1}{\mathcal{L}_{\text{int}}} \frac{1}{\text{BR}} \frac{N(p_{T, \text{chjet}})}{\Delta\eta_{\text{jet}}\Delta p_{T, \text{chjet}}}, \quad (4)$$

where $N(p_{T, \text{chjet}})$ is the measured yield in each $p_{T, \text{chjet}}$ interval corrected for the acceptance, reconstruction efficiency, b-hadron feed-down contribution, and unfolded for the detector effects. The $\Delta p_{T, \text{chjet}}$ is the bin width and $\Delta\eta_{\text{jet}} = 1.8 - 2R$ is the jet reconstruction acceptance, where R is the jet resolution parameter. Finally, \mathcal{L}_{int} is the integrated luminosity and BR is the branching ratio of the considered D^0 -meson decay channel.

The $p_{T, \text{chjet}}$ -differential cross sections of D^0 jets in pp collisions for $R = 0.2, 0.4$, and 0.6 are shown in Fig. 7 for $\sqrt{s} = 13$ TeV (left) and for $\sqrt{s} = 5.02$ TeV (right). They are compared to PYTHIA 8 and POWHEG + PYTHIA 8 predictions. The $p_{T, \text{chjet}}$ -differential cross section for $R = 0.3$ and its comparisons to theoretical predictions are shown in the appendix in Fig. A.1. The jets are required to have in their constituents a D^0 meson with $p_{T, D^0} > 2$ GeV/c as the D^0 -meson reconstruction efficiency falls rapidly at lower p_{T, D^0} and excluding $p_{T, D^0} < 2$ GeV/c helps in avoiding large fluctuations in the $p_{T, \text{chjet}}$ spectra. A previous study at $\sqrt{s} = 7$ TeV [18] showed that a lower bound selection on the D^0 -meson p_T of $p_{T, D^0} > 3$ GeV/c introduced a minimal fragmentation bias on the reported D^0 -jet $p_{T, \text{chjet}}$ -differential

cross sections above 5 GeV/ c . Therefore, a selection of $p_{T,D^0} > 2$ GeV/ c should have a smaller effect on the same reported range of $p_{T, \text{chjet}}$ spectra. In this analysis, the maximum transverse momentum was $p_{T,D^0} = 36$ GeV/ c for the D⁰ mesons and $p_{T, \text{chjet}} = 50$ GeV/ c for the charged jets. The same requirements on the D⁰-meson p_T were applied in the simulations.

The results are compared to predictions of the Monash-2013 tune [70] of the PYTHIA 8.210 [48] event generator with HardQCD processes. It is based on leading order pQCD calculations of matrix elements of parton-level hard scatterings and a leading order parton shower. The final state evolution is combined with the initial-state radiation and multiparton interactions. The Lund string model [71, 72] is used for the hadronisation. It overpredicts the data for all three values of the jet resolution parameter R with the discrepancy being larger at $\sqrt{s} = 13$ TeV. Incorporating SoftQCD and inelastic non-diffractive processes and colour reconnection beyond the leading-colour approximation [73] to the aforementioned PYTHIA 8 tune, denoted as PYTHIA 8 SoftQCD Mode 2, improves the agreement with the data. However, in this case the model underpredicts the measurements at $p_{T, \text{chjet}} \lesssim 10$ GeV/ c .

The POWHEG + PYTHIA 8 simulation interfaces NLO pQCD POWHEG [49, 63] calculations with the PYTHIA 8 [48] MC parton shower within the POWHEG Box framework [50]. The heavy-flavour process (hvq) [74] implementation of the POWHEG framework was chosen. The outgoing partons from POWHEG are passed to PYTHIA 8 event-by-event to simulate the subsequent parton shower, hadronisation and generation of the underlying event. The following simulation settings were used: CT10NLO set of the parton distribution function, the renormalisation and factorisation scales were set to $\mu_R = \mu_F = \mu_0 = \sqrt{m_c^2 + p_T^2}$, and the default charm-quark mass was 1.5 GeV/ c^2 . The theoretical uncertainties were estimated by varying the simulation parameters. The largest uncertainties originate from doubling or halving the factorisation and renormalisation scales. Additionally, the charm-quark mass was varied between 1.3 GeV/ c^2 and 1.7 GeV/ c^2 . The POWHEG + PYTHIA 8 calculations describe the measured cross sections within the experimental and theoretical uncertainties. For $p_{T, \text{chjet}} > 14$ GeV/ c (20 GeV/ c) the central values of the predictions agree with the data at $\sqrt{s} = 5.02$ TeV ($\sqrt{s} = 13$ TeV). At lower $p_{T, \text{chjet}}$ the experimental results are close to the upper bands of the POWHEG + PYTHIA 8 calculations and, as in the case of the PYTHIA 8 predictions, the agreement is better at $\sqrt{s} = 5.02$ TeV than at $\sqrt{s} = 13$ TeV. The low- $p_{T, \text{chjet}}$ region is particularly difficult to describe theoretically due to the large contribution from various non-perturbative effects.

In addition, the energy dependence of the $p_{T, \text{chjet}}$ -differential cross section of D⁰ jets was studied from the ratio of $\sqrt{s} = 13$ TeV to $\sqrt{s} = 5.02$ TeV cross sections, shown for different jet resolution parameters R in Fig. 8. The measured ratios indicate a hardening of the $p_{T, \text{chjet}}$ spectra with increasing centre-of-mass energy. Both PYTHIA 8 settings describe the data well within the current uncertainties for all jet resolution parameters R . The PYTHIA 8 with SoftQCD and Mode 2 tune describes the data slightly better. The POWHEG + PYTHIA 8 simulation underestimates the measured cross section ratios, with the data being on the upper edge of the theory uncertainty band.

5.2 Resolution parameter dependence of D⁰-jet cross section

A comparison of D⁰ jets with different resolution parameters can help in exploring the shower development. It provides insights into the interplay between perturbative and non-perturbative effects. Figure 9 shows the ratios of $p_{T, \text{chjet}}$ -differential cross sections of D⁰ jets reconstructed with resolution parameter $R = 0.2$ with respect to $R = 0.4$ and 0.6 for collision energies at $\sqrt{s} = 13$ TeV (left) and $\sqrt{s} = 5.02$ TeV (right). Statistical uncertainties are treated as fully uncorrelated and summed in quadrature, thus they are overestimated. To determine the theoretical uncertainties for cross section ratios between two jet radii in the POWHEG framework, the renormalisation and factorisation scales and the charm-quark mass were varied simultaneously. The maximum upward and downward variations were used as the uncertainty band.

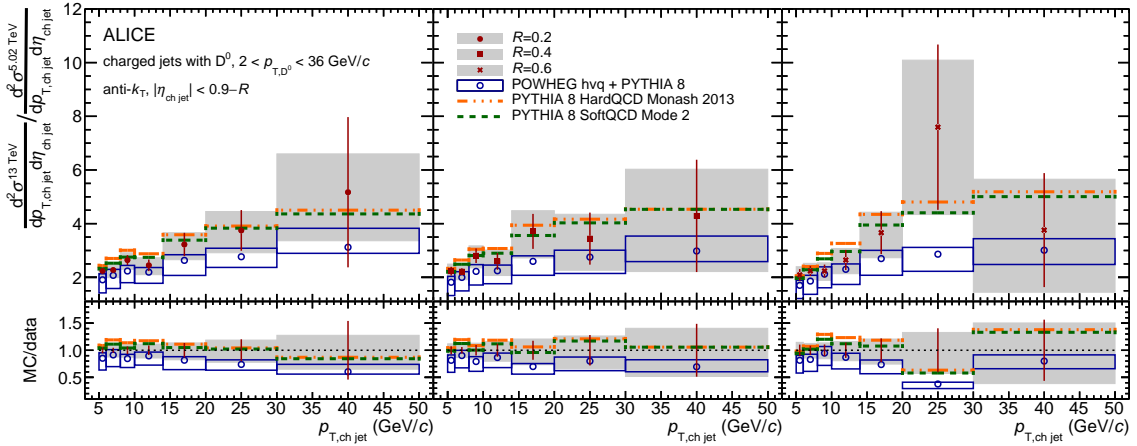


Figure 8: Top: ratios of $p_{T, \text{chjet}}$ -differential cross section of charm jets tagged with D^0 mesons in pp collisions at $\sqrt{s} = 13$ TeV to $\sqrt{s} = 5.02$ TeV for $R = 0.2$ (left), $R = 0.4$ (centre), and $R = 0.6$ (right) compared to PYTHIA 8 HardQCD Monash 2013 (dash-dotted lines), PYTHIA 8 SoftQCD Mode 2 (dashed lines), and POWHEG hvq + PYTHIA 8 (open circles) predictions. The shaded bands indicate the systematic uncertainty on the cross section ratios while open boxes represent the theoretical uncertainties on the POWHEG predictions. Bottom: ratios of MC predictions to the data.

The observed departure from unity of the cross section ratios can be interpreted by the emission of QCD radiation. Both $\sigma(R = 0.2)/\sigma(R = 0.4)$ and $\sigma(R = 0.2)/\sigma(R = 0.6)$ ratios for the two collision energies decrease with increasing $p_{T, \text{chjet}}$ and for $p_{T, \text{chjet}} > 10$ GeV/c the ratios become independent of $p_{T, \text{chjet}}$ within the uncertainties. The shapes are qualitatively described by the PYTHIA 8 and POWHEG + PYTHIA 8 predictions.

However, in the $p_{T, \text{chjet}}$ interval 5–10 GeV/c, POWHEG + PYTHIA 8 calculations overestimate the data with the discrepancy being larger for the $\sigma(R = 0.2)/\sigma(R = 0.6)$ ratio, which is expected to be more sensitive to the underlying event contribution. The PYTHIA 8 predictions with the Monash and Mode 2 tunes agree well with the data within the uncertainties, where the largest deviations from the data are at low $p_{T, \text{chjet}}$ for $\sqrt{s} = 13$ TeV and $R = 0.6$. The differences seen between the predictions of the two PYTHIA 8 tunes in the $p_{T, \text{chjet}}$ -differential cross sections largely cancel in the ratios of results with different R parameters.

5.3 D^0 -jet fraction of inclusive jets

Figure 10 shows the fraction of D^0 jets with respect to charged-particle inclusive jets in pp collisions at $\sqrt{s} = 5.02$ TeV for different jet resolution parameters $R = 0.2, 0.4$, and 0.6 . The production cross sections of the inclusive jets used as a reference here are taken from a previous measurement by ALICE reported in Ref. [69]. Since the data taking periods are different for the inclusive jet measurements compared to the current one, all the uncertainties were considered as uncorrelated.

The fraction of D^0 jets tends to increase with increasing $p_{T, \text{chjet}}$ in the kinematic range $5 < p_{T, \text{chjet}} < 10$ GeV/c for all jet radii. However, the fraction decreases with increasing R , from a range of 0.05–0.07 at $R = 0.2$ to a range of 0.015–0.04 at $R = 0.6$. The D^0 -jet fraction for $R = 0.3$ is shown in the appendix in Fig. A.2. In the range of $p_{T, \text{chjet}} > 10$ GeV/c, the $p_{T, \text{chjet}}$ dependence tends to flatten out within uncertainties due to the hardening of the jets. The D^0 -jet fractions follow the trend set by PYTHIA 8 results with Monash tune and agree with them quite well. The POWHEG + PYTHIA 8 calculations slightly underestimate the data at lower $p_{T, \text{chjet}}$ while agreeing within uncertainties at higher $p_{T, \text{chjet}}$.

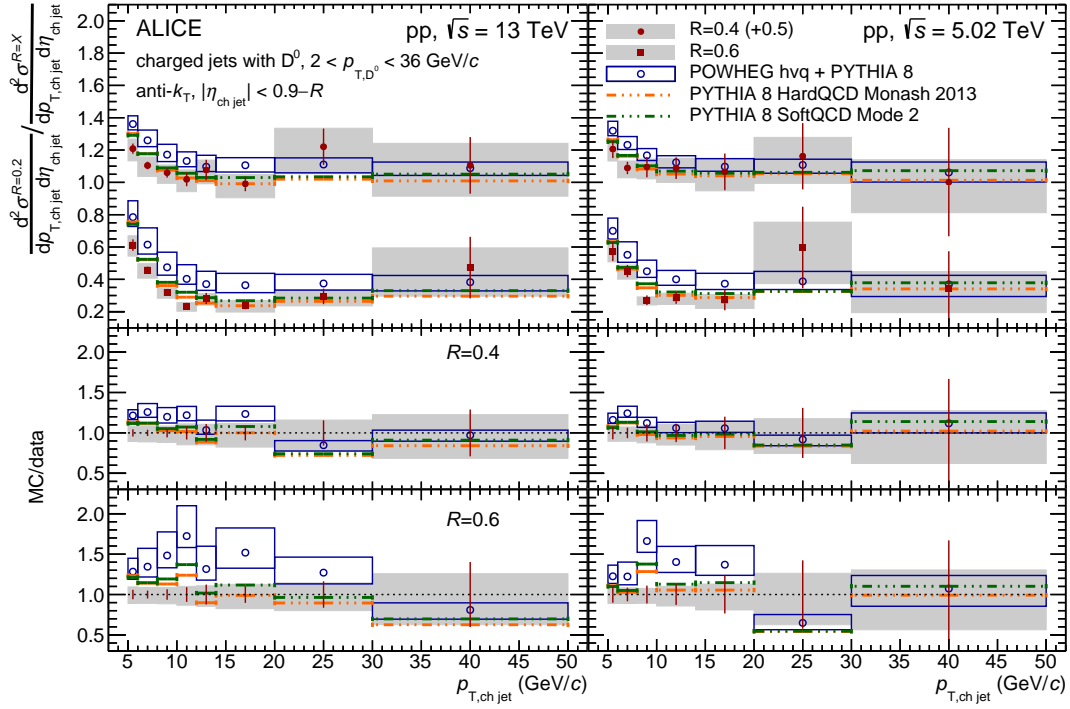


Figure 9: Top: ratios of $p_{T, \text{ch jet}}$ -differential cross section of charm jets tagged with D^0 mesons for different R : $\sigma(R = 0.2)/\sigma(R = 0.4)$ (circles, shifted up by 0.5) and $\sigma(R = 0.2)/\sigma(R = 0.6)$ (squares) in pp collisions at $\sqrt{s} = 13$ TeV (left) and $\sqrt{s} = 5.02$ TeV (right) compared to PYTHIA 8 HardQCD Monash 2013 (dash-dotted lines), PYTHIA 8 SoftQCD Mode 2 (dashed lines), and POWHEG hvq + PYTHIA 8 (open circles) predictions. The shaded bands indicate the systematic uncertainty on the cross section ratios while open boxes represent the theoretical uncertainties on the POWHEG predictions. Bottom: ratios of MC predictions to the data for $\sigma(R = 0.2)/\sigma(R = 0.4)$ and $\sigma(R = 0.2)/\sigma(R = 0.6)$, respectively.

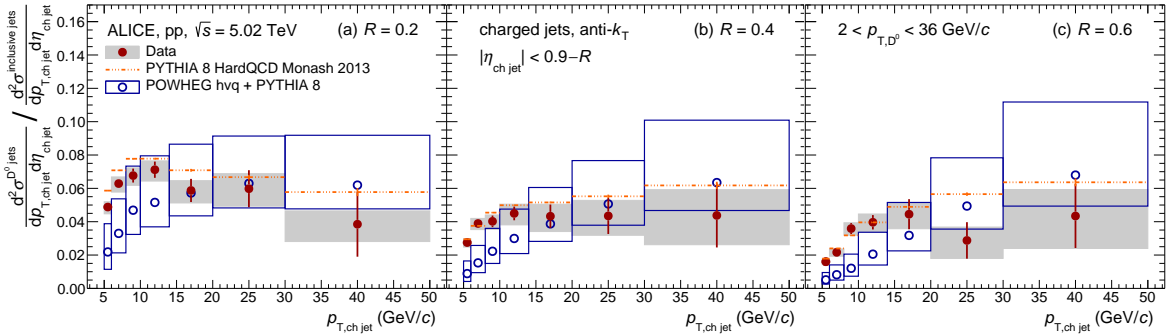


Figure 10: The fraction of D^0 jets over inclusive charged-particle jets in pp collisions at $\sqrt{s} = 5.02$ TeV for (a) $R = 0.2$, (b) $R = 0.4$, and (c) $R = 0.6$ compared to PYTHIA 8 HardQCD Monash 2013 (dash-dotted lines) and POWHEG hvq + PYTHIA 8 (open circles) predictions. The shaded bands indicate the systematic uncertainty on the data cross section ratios while the open boxes represent the theoretical uncertainties on the POWHEG predictions.

5.4 Jet momentum fraction

The fraction of jet momentum carried by the D^0 meson can provide insight into the charm-quark fragmentation. The $z_{\parallel}^{\text{ch}}$ -differential yield, $d^2N/dz_{\parallel}^{\text{ch}} d\eta_{\text{jet}}$, was calculated in a manner analogous to the calculation

of $p_{T,\text{chjet}}$ -differential cross section (see 4). It was then self-normalised in each $p_{T,\text{chjet}}$ interval by the integral of the measured $z_{\parallel}^{\text{ch}}$ distribution in the corresponding $p_{T,\text{chjet}}$ interval to obtain the presented $z_{\parallel}^{\text{ch}}$ probability density distributions

$$\frac{1}{N} \frac{d^2N}{dz_{\parallel}^{\text{ch}} d\eta_{\text{jet}}}(z_{\parallel}^{\text{ch}}, p_{T,\text{chjet}}) = \frac{1}{N(p_{T,\text{chjet}})} \frac{N(z_{\parallel}^{\text{ch}}, p_{T,\text{chjet}})}{\Delta\eta_{\text{jet}} \Delta z_{\parallel}^{\text{ch}}}. \quad (5)$$

This normalisation was applied in order to better compare the shape of the distributions among each other and to different model predictions. Figures 11 and 12 show the $z_{\parallel}^{\text{ch}}$ distributions in four different intervals of $p_{T,\text{chjet}}$ for $\sqrt{s} = 13$ TeV and $\sqrt{s} = 5.02$ TeV, respectively. The distributions for $R = 0.3$ D⁰ jets at $\sqrt{s} = 5.02$ TeV are shown in Fig. A.3. A $p_{T,\text{chjet}}$ -dependent minimum D⁰-meson p_T requirement had to be applied due to the limited number of candidates in some momentum intervals. For $R = 0.2$, these were $p_{T,D^0} > 2, 4, 5,$ and 10 GeV/ c in the $p_{T,\text{chjet}}$ ranges $5 < p_{T,\text{chjet}} < 7, 7 < p_{T,\text{chjet}} < 10, 10 < p_{T,\text{chjet}} < 15,$ and $15 < p_{T,\text{chjet}} < 50$ GeV/ c , respectively. For $R = 0.4$ and 0.6 , the respective required selections on the minimum p_{T,D^0} were: $2, 3, 5,$ and 5 GeV/ c . The same kinematic conditions were adopted in the model calculations.

For D⁰ jets with $5 < p_{T,\text{chjet}} < 15$ GeV/ c and reconstructed with $R = 0.2$, a peak at $z_{\parallel}^{\text{ch}} \approx 1$ is visible, for both $\sqrt{s} = 5.02$ TeV and $\sqrt{s} = 13$ TeV. The peak contains jets whose only constituent is the tagged D⁰ meson and it disappears at larger R and higher $p_{T,\text{chjet}}$ intervals where the fraction of these single-constituent jets becomes much smaller. For a given $p_{T,\text{chjet}}$ interval, a softening of the fragmentation ($z_{\parallel}^{\text{ch}}$) is visible with increasing R . The change in the $z_{\parallel}^{\text{ch}}$ distribution shape with increasing $p_{T,\text{chjet}}$ is significant only for $R = 0.4$, with a trend that is similar to that reported in previous ALICE studies at $\sqrt{s} = 7$ TeV [18].

The measured $z_{\parallel}^{\text{ch}}$ distributions are compared to the predictions of the same models used for the $p_{T,\text{chjet}}$ -differential cross section. Overall, a good agreement between PYTHIA 8 results with both Monash and Mode 2 tunes and the data is observed within the uncertainties for $7 < p_{T,\text{chjet}} < 50$ GeV/ c at both collision energies. A hint of a softer fragmentation in the lowest $p_{T,\text{chjet}}$ interval, $5 < p_{T,\text{chjet}} < 7$ GeV/ c , is visible in the data compared to the PYTHIA 8 predictions. The differences in the $z_{\parallel}^{\text{ch}}$ distribution shape predicted by the default PYTHIA 8 Monash 2013 tune and the SoftQCD Mode 2 are very small, with a slightly harder fragmentation predicted by the former at low $p_{T,\text{chjet}}$ and smaller R . Similarly, POWHEG + PYTHIA 8 describes the data well above $p_{T,\text{chjet}} > 7$ (10) GeV/ c at $\sqrt{s} = 5.02$ TeV ($\sqrt{s} = 13$ TeV) while it predicts a harder fragmentation at lower $p_{T,\text{chjet}}$. The discrepancy between the data and POWHEG + PYTHIA 8 predictions in these lower $p_{T,\text{chjet}}$ ranges in the $z_{\parallel}^{\text{ch}}$ distribution shape is larger than in the case of the PYTHIA 8 event generator. It is particularly significant at $\sqrt{s} = 13$ TeV in the interval $5 < p_{T,\text{chjet}} < 10$ GeV/ c for jets reconstructed with $R = 0.6$ and 0.4 and for $5 < p_{T,\text{chjet}} < 7$ GeV/ c with $R = 0.2$. The discrepancy is larger for larger R .

6 Summary

In this paper, studies of the production of charm jets tagged with fully reconstructed D⁰ mesons, using data obtained from proton–proton collisions at $\sqrt{s} = 5.02$ TeV and $\sqrt{s} = 13$ TeV with the ALICE detector at the CERN LHC, were presented. The measurements were carried out for charged-particle jets reconstructed with different resolution parameters, i.e. $R = 0.2, 0.4, 0.6$. The new ALICE results shown in this paper have better precision for the studied observables and are performed more differentially owing to larger data samples of pp collisions at $\sqrt{s} = 13$ and 5.02 TeV collected by ALICE compared to the results obtained at $\sqrt{s} = 7$ TeV [18]. They are differential in $p_{T,\text{chjet}}$ and double differential in $z_{\parallel}^{\text{ch}}$ and $p_{T,\text{chjet}}$, and are compared to predictions obtained with the PYTHIA 8 event generator with the Monash tune as well as with the Mode 2 tune (implementing colour reconnection beyond the leading-colour approximation), and to predictions obtained by coupling the POWHEG NLO event generator to the PYTHIA 8 parton shower.

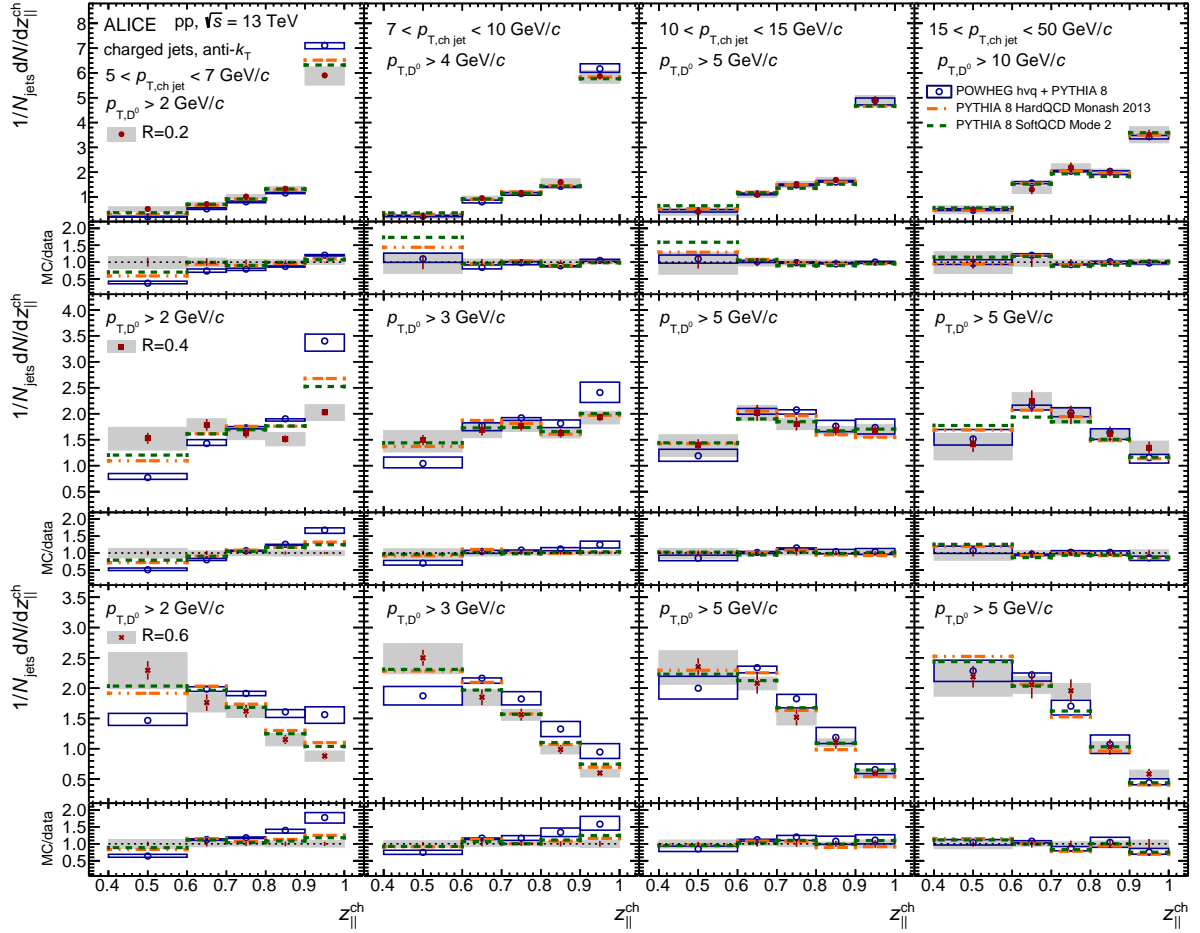


Figure 11: Distributions of $z_{\parallel}^{\text{ch}}$ -differential yield of charm jets tagged with D^0 mesons normalised by the number of D^0 jets within each distribution in pp collisions at $\sqrt{s} = 13$ TeV in four jet- p_{T} intervals $5 < p_{\text{T,chjet}} < 7$ GeV/ c , $7 < p_{\text{T,chjet}} < 10$ GeV/ c , $10 < p_{\text{T,chjet}} < 15$ GeV/ c , and $15 < p_{\text{T,chjet}} < 50$ GeV/ c from left to right, respectively. Top, middle, and bottom rows represent jets with $R = 0.2$, 0.4 , and 0.6 , respectively. They are compared to PYTHIA 8 HardQCD Monash 2013 (dash-dotted lines), PYTHIA 8 SoftQCD Mode 2 (dashed lines), and POWHEG hvq + PYTHIA 8 (open circles) predictions. The shaded bands indicate the systematic uncertainty on the distributions. Bottom panels present ratios of MC predictions to the data.

The PYTHIA 8 predictions with the SoftQCD and Mode 2 tune settings provide the best description of the $p_{\text{T,chjet}}$ -differential cross sections for both collision energies and all resolution parameters. Within the experimental and theoretical uncertainties, the measurements are also in agreement with the POWHEG + PYTHIA 8 calculations. Cross section ratios between $\sqrt{s} = 13$ and 5.02 TeV increase with increasing $p_{\text{T,chjet}}$, indicating a hardening of the spectrum as the collision energy rises. The cross section ratios between different jet radii $\sigma(R = 0.2)/\sigma(R = 0.4, 0.6)$ fall sharply with $p_{\text{T,chjet}}$ and then flatten out for $p_{\text{T,chjet}} > 10$ GeV/ c . Low- $p_{\text{T,chjet}}$ measurements for different R values can constrain pQCD, hadronisation, and underlying event (UE) effects in models. Studies for smaller R values are more sensitive to non-perturbative hadronisation effects, while contributions from the UE are more important for large R . The ratios are well described by the PYTHIA 8 predictions and are systematically overpredicted by the POWHEG + PYTHIA 8 calculations, especially for $p_{\text{T,chjet}} < 20$ GeV/ c and $\sqrt{s} = 13$ TeV.

The probability density distributions of the jet momentum fraction carried by the constituent D^0 meson, $z_{\parallel}^{\text{ch}}$, hint at a softer fragmentation in data when compared to model predictions in the low $p_{\text{T,chjet}}$ re-

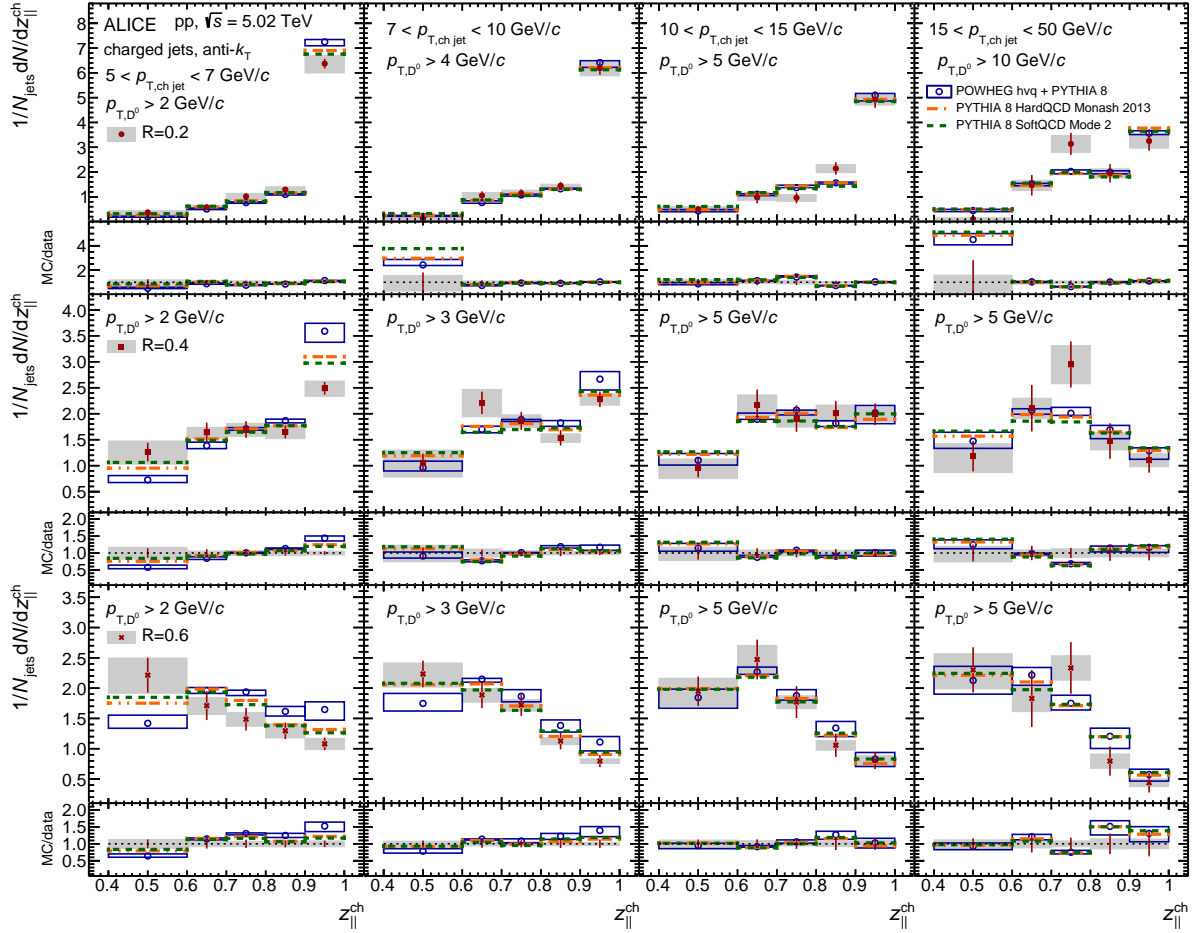


Figure 12: Distributions of $z_{\parallel}^{\text{ch}}$ -differential yield of charm jets tagged with D⁰ mesons and normalised by the number of D⁰ jets within each distribution in pp collisions at $\sqrt{s} = 5.02$ TeV in four $p_{T,\text{chjet}}$ intervals $5 < p_{T,\text{chjet}} < 7$ GeV/c, $7 < p_{T,\text{chjet}} < 10$ GeV/c, $10 < p_{T,\text{chjet}} < 15$ GeV/c, and $15 < p_{T,\text{chjet}} < 50$ GeV/c from left to right, respectively. Top, middle, and bottom rows represent jets with $R = 0.2$, 0.4 , and 0.6 , respectively. They are compared to PYTHIA 8 HardQCD Monash 2013 (dash-dotted lines), PYTHIA 8 SoftQCD Mode 2 (dashed lines), and POWHEG hvq + PYTHIA 8 (open circles) predictions. The shaded bands indicate the systematic uncertainty on the distributions. Bottom panels present ratios of MC predictions to the data.

gion and for larger jet radii. This disagreement is more prominent for NLO predictions obtained from POWHEG + PYTHIA 8 than PYTHIA 8 predictions. For $p_{T,\text{chjet}} > 7$ GeV/c, the agreement between data and the calculations is good.

Despite these discrepancies at low $p_{T,\text{chjet}}$, a generally good description of the main features of the data is obtained with MC event generators and pQCD calculations in most of the measured kinematic range, indicating that the charm-quark production, fragmentation and hadronisation are under control. Therefore, these models can serve as a good theoretical baseline for studies in p–Pb and Pb–Pb collisions. The reported $z_{\parallel}^{\text{ch}}$ distributions also serve as an important input for the global fit analyses that aim to constrain the gluon fragmentation functions. Furthermore, the results from pp collisions at $\sqrt{s} = 5.02$ TeV are at the same centre-of-mass energy as p–Pb and Pb–Pb collision data and can be used as a reference for studies of charm-jet production and fragmentation modifications in the QGP medium and cold nuclear matter effects in p–Pb collisions.

Acknowledgements

The ALICE Collaboration would like to thank all its engineers and technicians for their invaluable contributions to the construction of the experiment and the CERN accelerator teams for the outstanding performance of the LHC complex. The ALICE Collaboration gratefully acknowledges the resources and support provided by all Grid centres and the Worldwide LHC Computing Grid (WLCG) collaboration. The ALICE Collaboration acknowledges the following funding agencies for their support in building and running the ALICE detector: A. I. Alikhanyan National Science Laboratory (Yerevan Physics Institute) Foundation (ANSL), State Committee of Science and World Federation of Scientists (WFS), Armenia; Austrian Academy of Sciences, Austrian Science Fund (FWF): [M 2467-N36] and Nationalstiftung für Forschung, Technologie und Entwicklung, Austria; Ministry of Communications and High Technologies, National Nuclear Research Center, Azerbaijan; Conselho Nacional de Desenvolvimento Científico e Tecnológico (CNPq), Financiadora de Estudos e Projetos (Finep), Fundação de Amparo à Pesquisa do Estado de São Paulo (FAPESP) and Universidade Federal do Rio Grande do Sul (UFRGS), Brazil; Bulgarian Ministry of Education and Science, within the National Roadmap for Research Infrastructures 2020-2027 (object CERN), Bulgaria; Ministry of Education of China (MOEC), Ministry of Science & Technology of China (MSTC) and National Natural Science Foundation of China (NSFC), China; Ministry of Science and Education and Croatian Science Foundation, Croatia; Centro de Aplicaciones Tecnológicas y Desarrollo Nuclear (CEADEN), Cubaenergía, Cuba; Ministry of Education, Youth and Sports of the Czech Republic, Czech Republic; The Danish Council for Independent Research | Natural Sciences, the VILLUM FONDEN and Danish National Research Foundation (DNRF), Denmark; Helsinki Institute of Physics (HIP), Finland; Commissariat à l’Energie Atomique (CEA) and Institut National de Physique Nucléaire et de Physique des Particules (IN2P3) and Centre National de la Recherche Scientifique (CNRS), France; Bundesministerium für Bildung und Forschung (BMBF) and GSI Helmholtzzentrum für Schwerionenforschung GmbH, Germany; General Secretariat for Research and Technology, Ministry of Education, Research and Religions, Greece; National Research, Development and Innovation Office, Hungary; Department of Atomic Energy Government of India (DAE), Department of Science and Technology, Government of India (DST), University Grants Commission, Government of India (UGC) and Council of Scientific and Industrial Research (CSIR), India; National Research and Innovation Agency - BRIN, Indonesia; Istituto Nazionale di Fisica Nucleare (INFN), Italy; Japanese Ministry of Education, Culture, Sports, Science and Technology (MEXT) and Japan Society for the Promotion of Science (JSPS) KAKENHI, Japan; Consejo Nacional de Ciencia (CONACYT) y Tecnología, through Fondo de Cooperación Internacional en Ciencia y Tecnología (FONCICYT) and Dirección General de Asuntos del Personal Académico (DGAPA), Mexico; Nederlandse Organisatie voor Wetenschappelijk Onderzoek (NWO), Netherlands; The Research Council of Norway, Norway; Commission on Science and Technology for Sustainable Development in the South (COMSATS), Pakistan; Pontificia Universidad Católica del Perú, Peru; Ministry of Education and Science, National Science Centre and WUT ID-UB, Poland; Korea Institute of Science and Technology Information and National Research Foundation of Korea (NRF), Republic of Korea; Ministry of Education and Scientific Research, Institute of Atomic Physics, Ministry of Research and Innovation and Institute of Atomic Physics and University Politehnica of Bucharest, Romania; Ministry of Education, Science, Research and Sport of the Slovak Republic, Slovakia; National Research Foundation of South Africa, South Africa; Swedish Research Council (VR) and Knut & Alice Wallenberg Foundation (KAW), Sweden; European Organization for Nuclear Research, Switzerland; Suranaree University of Technology (SUT), National Science and Technology Development Agency (NSTDA), Thailand Science Research and Innovation (TSRI) and National Science, Research and Innovation Fund (NSRF), Thailand; Turkish Energy, Nuclear and Mineral Research Agency (TENMAK), Turkey; National Academy of Sciences of Ukraine, Ukraine; Science and Technology Facilities Council (STFC), United Kingdom; National Science Foundation of the United States of America (NSF) and United States Department of Energy, Office of Nuclear Physics (DOE NP), United States of America. In addition, individual groups or members have received sup-

port from: Marie Skłodowska Curie, Strong 2020 - Horizon 2020, European Research Council (grant nos. 824093, 896850, 950692), European Union; Academy of Finland (Center of Excellence in Quark Matter) (grant nos. 346327, 346328), Finland; Programa de Apoyos para la Superación del Personal Académico, UNAM, Mexico.

References

- [1] M. Cacciari, P. Nason, and R. Vogt, “QCD predictions for charm and bottom production at RHIC”, *Phys. Rev. Lett.* **95** (2005) 122001, arXiv:hep-ph/0502203 [hep-ph].
- [2] B. A. Kniehl, G. Kramer, I. Schienbein, and H. Spiesberger, “Inclusive Charmed-Meson Production at the CERN LHC”, *Eur. Phys. J.* **C72** (2012) 2082, arXiv:1202.0439 [hep-ph].
- [3] R. Maciula and A. Szczurek, “Open charm production at the LHC - k_T -factorization approach”, *Phys. Rev.* **D87** (2013) 094022, arXiv:1301.3033 [hep-ph].
- [4] M. Cacciari, M. Greco, and P. Nason, “The p_T spectrum in heavy flavor hadroproduction”, *JHEP* **05** (1998) 007, arXiv:hep-ph/9803400 [hep-ph].
- [5] M. Benzke, M. V. Garzelli, B. Kniehl, G. Kramer, S. Moch, and G. Sigl, “Prompt neutrinos from atmospheric charm in the general-mass variable-flavor-number scheme”, *JHEP* **12** (2017) 021, arXiv:1705.10386 [hep-ph].
- [6] I. Helenius and H. Paukkunen, “Revisiting the D-meson hadroproduction in general-mass variable flavour number scheme”, *JHEP* **05** (2018) 196, arXiv:1804.03557 [hep-ph].
- [7] UA1 Collaboration, C. Albajar *et al.*, “Beauty Production at the CERN $p\bar{p}$ Collider”, *Phys. Lett. B* **186** (1987) 237–246.
- [8] CDF Collaboration, T. Aaltonen *et al.*, “Measurement of the b-Hadron Production Cross Section Using Decays to $\mu^- D^0 X$ Final States in $p\bar{p}$ Collisions at $\sqrt{s} = 1.96$ TeV”, *Phys. Rev. D* **79** (2009) 092003, arXiv:0903.2403 [hep-ex].
- [9] STAR Collaboration, L. Adamczyk *et al.*, “Measurements of D^0 and D^* Production in $p + p$ Collisions at $\sqrt{s} = 200$ GeV”, *Phys. Rev.* **D86** (2012) 072013, arXiv:1204.4244 [nucl-ex].
- [10] PHENIX Collaboration, A. Adare *et al.*, “Measurements of e^+e^- pairs from open heavy flavor in $p+p$ and $d+A$ collisions at $\sqrt{s_{NN}} = 200$ GeV”, *Phys. Rev. C* **96** (2017) 024907, arXiv:1702.01084 [nucl-ex].
- [11] ALICE Collaboration, S. Acharya *et al.*, “Measurement of beauty and charm production in pp collisions at $\sqrt{s} = 5.02$ TeV via non-prompt and prompt D mesons”, *JHEP* **05** (2021) 220, arXiv:2102.13601 [nucl-ex].
- [12] ATLAS Collaboration, G. Aad *et al.*, “Measurement of $D^{*\pm}$, D^\pm and D_s^\pm meson production cross sections in pp collisions at $\sqrt{s} = 7$ TeV with the ATLAS detector”, *Nucl. Phys. B* **907** (2016) 717–763, arXiv:1512.02913 [hep-ex].
- [13] CMS Collaboration, A. M. Sirunyan *et al.*, “Production of Λ_c^+ baryons in proton-proton and lead-lead collisions at $\sqrt{s_{NN}} = 5.02$ TeV”, *Phys. Lett. B* **803** (2020) 135328, arXiv:1906.03322 [hep-ex].
- [14] LHCb Collaboration, R. Aaij *et al.*, “Measurements of prompt charm production cross-sections in pp collisions at $\sqrt{s} = 13$ TeV”, *JHEP* **03** (2016) 159, arXiv:1510.01707 [hep-ex]. Erratum: *JHEP* **09** (2016) 013; Erratum: *JHEP* **05** (2017) 074.

- [15] D. P. Anderle, T. Kaufmann, M. Stratmann, F. Ringer, and I. Vitev, “Using hadron-in-jet data in a global analysis of D^* fragmentation functions”, *Phys. Rev.* **D96** (2017) 034028, arXiv:1706.09857 [hep-ph].
- [16] H. T. Li, Z. L. Liu, and I. Vitev, “Heavy flavor jet production and substructure in electron-nucleus collisions”, *Phys. Lett. B* **827** (2022) 137007, arXiv:2108.07809 [hep-ph].
- [17] CMS Collaboration, A. M. Sirunyan *et al.*, “Measurements of the charm jet cross section and nuclear modification factor in pPb collisions at $\sqrt{s_{NN}} = 5.02$ TeV”, *Phys. Lett.* **B772** (2017) 306–329, arXiv:1612.08972 [nucl-ex].
- [18] ALICE Collaboration, S. Acharya *et al.*, “Measurement of the production of charm jets tagged with D^0 mesons in pp collisions at $\sqrt{s} = 7$ TeV”, *JHEP* **08** (2019) 133, arXiv:1905.02510 [nucl-ex].
- [19] CMS Collaboration, S. Chatrchyan *et al.*, “Inclusive b -jet production in pp collisions at $\sqrt{s} = 7$ TeV”, *JHEP* **04** (2012) 084, arXiv:1202.4617 [hep-ex].
- [20] ATLAS Collaboration, G. Aad *et al.*, “Measurement of $D^{*+/-}$ meson production in jets from pp collisions at $\sqrt{s} = 7$ TeV with the ATLAS detector”, *Phys. Rev.* **D85** (2012) 052005, arXiv:1112.4432 [hep-ex].
- [21] ATLAS Collaboration, G. Aad *et al.*, “Measurement of b -quark fragmentation properties in jets using the decay $B^\pm \rightarrow J/\psi K^\pm$ in pp collisions at $\sqrt{s} = 13$ TeV with the ATLAS detector”, *JHEP* **12** (2021) 131, arXiv:2108.11650 [hep-ex].
- [22] ALICE Collaboration, S. Acharya *et al.*, “Measurement of inclusive charged-particle b -jet production in pp and p-Pb collisions at $\sqrt{s_{NN}} = 5.02$ TeV”, *JHEP* **01** (2022) 178, arXiv:2110.06104 [nucl-ex].
- [23] STAR Collaboration, B. I. Abelev *et al.*, “Measurement of D^* Mesons in Jets from p+p Collisions at $\sqrt{s} = 200$ GeV”, *Phys. Rev.* **D79** (2009) 112006, arXiv:0901.0740 [hep-ex].
- [24] UA1 Collaboration, C. Albajar *et al.*, “A Study of the D^* content of jets at the CERN $p\bar{p}$ collider”, *Phys. Lett.* **B244** (1990) 566–572.
- [25] CDF Collaboration, F. Abe *et al.*, “A measurement of D^* production in jets from $\bar{p}p$ collisions at $\sqrt{s} = 1.8$ TeV”, *Phys. Rev. Lett.* **64** (1990) 348.
- [26] Y.-T. Chien, Z.-B. Kang, F. Ringer, I. Vitev, and H. Xing, “Jet fragmentation functions in proton-proton collisions using soft-collinear effective theory”, *JHEP* **05** (2016) 125, arXiv:1512.06851 [hep-ph].
- [27] ZEUS Collaboration, S. Chekanov *et al.*, “Measurement of the charm fragmentation function in D^* photoproduction at HERA”, *JHEP* **04** (2009) 082, arXiv:0901.1210 [hep-ex].
- [28] Belle Collaboration, R. Seuster *et al.*, “Charm hadrons from fragmentation and B decays in e^+e^- annihilation at $s^{*1/2} = 10.6$ -GeV”, *Phys. Rev. D* **73** (2006) 032002, arXiv:hep-ex/0506068.
- [29] W. Busza, K. Rajagopal, and W. van der Schee, “Heavy Ion Collisions: The Big Picture, and the Big Questions”, *Ann. Rev. Nucl. Part. Sci.* **68** (2018) 339–376, arXiv:1802.04801 [hep-ph].
- [30] HotQCD Collaboration, A. Bazavov *et al.*, “Chiral crossover in QCD at zero and non-zero chemical potentials”, *Phys. Lett. B* **795** (2019) 15–21, arXiv:1812.08235 [hep-lat].

- [31] S. Borsanyi, Z. Fodor, J. N. Guenther, R. Kara, *et al.*, “QCD Crossover at Finite Chemical Potential from Lattice Simulations”, *Phys. Rev. Lett.* **125** (2020) 052001, arXiv:2002.02821 [hep-lat].
- [32] H. Satz, “Colour deconfinement and quarkonium binding”, *Journal of Physics G: Nuclear and Particle Physics* **32** (2006) R25–R69.
- [33] U. W. Heinz and M. Jacob, “Evidence for a new state of matter: An Assessment of the results from the CERN lead beam program”, arXiv:nuc1-th/0002042.
- [34] **PHENIX** Collaboration, K. Adcox *et al.*, “Formation of dense partonic matter in relativistic nucleus-nucleus collisions at RHIC: Experimental evaluation by the PHENIX collaboration”, *Nucl. Phys. A* **757** (2005) 184–283, arXiv:nuc1-ex/0410003.
- [35] J. Aichelin, P. B. Gossiaux, and T. Gousset, “Radiative and Collisional Energy Loss of Heavy Quarks in Deconfined Matter”, *Acta Phys. Polon. B* **43** (2012) 655–662, arXiv:1201.4192 [nucl-th].
- [36] X. Dong, Y.-J. Lee, and R. Rapp, “Open Heavy-Flavor Production in Heavy-Ion Collisions”, *Ann. Rev. Nucl. Part. Sci.* **69** (2019) 417–445, arXiv:1903.07709 [nucl-ex].
- [37] **ALICE** Collaboration, B. Abelev *et al.*, “Suppression of high transverse momentum D mesons in central Pb-Pb collisions at $\sqrt{s_{NN}} = 2.76$ TeV”, *JHEP* **09** (2012) 112, arXiv:1203.2160 [nucl-ex].
- [38] **ALICE** Collaboration, J. Adam *et al.*, “Centrality dependence of high- p_T D meson suppression in Pb-Pb collisions at $\sqrt{s_{NN}} = 2.76$ TeV”, *JHEP* **11** (2015) 205, arXiv:1506.06604 [nucl-ex]. Erratum: *JHEP* **06** (2017) 032.
- [39] **ALICE** Collaboration, S. Acharya *et al.*, “Measurement of D^0 , D^+ , D^{*+} and D_s^+ production in Pb-Pb collisions at $\sqrt{s_{NN}} = 5.02$ TeV”, *JHEP* **10** (2018) 174, arXiv:1804.09083 [nucl-ex].
- [40] **STAR** Collaboration, J. Adam *et al.*, “Centrality and transverse momentum dependence of D^0 -meson production at mid-rapidity in Au+Au collisions at $\sqrt{s_{NN}} = 200$ GeV”, *Phys. Rev. C* **99** (2019) 034908, arXiv:1812.10224 [nucl-ex].
- [41] **CMS** Collaboration, A. M. Sirunyan *et al.*, “Nuclear modification factor of D^0 mesons in PbPb collisions at $\sqrt{s_{NN}} = 5.02$ TeV”, *Phys. Lett.* **B782** (2018) 474–496, arXiv:1708.04962 [nucl-ex].
- [42] A. Beraudo *et al.*, “Extraction of Heavy-Flavor Transport Coefficients in QCD Matter”, *Nucl. Phys. A* **979** (2018) 21–86, arXiv:1803.03824 [nucl-th].
- [43] S. Cao *et al.*, “Toward the determination of heavy-quark transport coefficients in quark-gluon plasma”, *Phys. Rev. C* **99** (2019) 054907, arXiv:1809.07894 [nucl-th].
- [44] **STAR** Collaboration, L. Adamczyk *et al.*, “Measurement of D^0 Azimuthal Anisotropy at Midrapidity in Au+Au Collisions at $\sqrt{s_{NN}}=200$ GeV”, *Phys. Rev. Lett.* **118** (2017) 212301, arXiv:1701.06060 [nucl-ex].
- [45] **ALICE** Collaboration, S. Acharya *et al.*, “Transverse-momentum and event-shape dependence of D-meson flow harmonics in Pb–Pb collisions at $\sqrt{s_{NN}} = 5.02$ TeV”, *Phys. Lett. B* **813** (2021) 136054, arXiv:2005.11131 [nucl-ex].

- [46] ALICE Collaboration, S. Acharya *et al.*, “Measurement of prompt D_s⁺-meson production and azimuthal anisotropy in Pb-Pb collisions at $\sqrt{s_{NN}} = 5.02$ TeV”, *Phys. Lett. B* **827** (2022) 136986, arXiv:2110.10006 [nucl-ex].
- [47] M. Dasgupta, F. A. Dreyer, G. P. Salam, and G. Soyez, “Inclusive jet spectrum for small-radius jets”, *JHEP* **06** (2016) 057, arXiv:1602.01110 [hep-ph].
- [48] T. Sjöstrand, S. Ask, J. R. Christiansen, *et al.*, “An introduction to PYTHIA 8.2”, *Comput. Phys. Commun.* **191** (2015) 159–177, arXiv:1410.3012 [hep-ph].
- [49] S. Frixione, P. Nason, and C. Oleari, “Matching NLO QCD computations with Parton Shower simulations: the POWHEG method”, *JHEP* **11** (2007) 070, arXiv:0709.2092 [hep-ph].
- [50] S. Alioli, P. Nason, C. Oleari, and E. Re, “A general framework for implementing NLO calculations in shower Monte Carlo programs: the POWHEG BOX”, *JHEP* **06** (2010) 043, arXiv:1002.2581 [hep-ph].
- [51] ALICE Collaboration, K. Aamodt *et al.*, “The ALICE experiment at the CERN LHC”, *Journal of Instrumentation* **3** (08, 2008) S08002.
- [52] ALICE Collaboration, B. B. Abelev *et al.*, “Performance of the ALICE Experiment at the CERN LHC”, *Int. J. Mod. Phys. A* **29** (2014) 1430044, arXiv:1402.4476 [nucl-ex].
- [53] ALICE Collaboration, S. Acharya *et al.*, “ALICE 2017 luminosity determination for pp collisions at $\sqrt{s} = 5$ TeV”, ALICE-PUBLIC-2018-014. <http://cds.cern.ch/record/2648933>.
- [54] ALICE Collaboration, S. Acharya *et al.*, “ALICE 2016-2017-2018 luminosity determination for pp collisions at $\sqrt{s} = 13$ TeV”, ALICE-PUBLIC-2021-005. <https://cds.cern.ch/record/2776672>.
- [55] T. Sjostrand, S. Mrenna, and P. Z. Skands, “PYTHIA 6.4 Physics and Manual”, *JHEP* **05** (2006) 026, arXiv:hep-ph/0603175.
- [56] P. Z. Skands, “Tuning Monte Carlo Generators: The Perugia Tunes”, *Phys. Rev. D* **82** (2010) 074018, arXiv:1005.3457 [hep-ph].
- [57] R. Brun, R. Hagelberg, M. Hansroul, and J. C. Lassalle, *Simulation program for particle physics experiments, GEANT: user guide and reference manual*. CERN, Geneva, 1978. <https://cds.cern.ch/record/118715>.
- [58] Particle Data Group Collaboration, P. A. Zyla *et al.*, “Review of Particle Physics”, *PTEP* **2020** (2020) 083C01.
- [59] ALICE Collaboration, S. Acharya *et al.*, “Measurement of D⁰, D⁺, D^{*+} and D_s⁺ production in pp collisions at $\sqrt{s} = 5.02$ TeV with ALICE”, *Eur. Phys. J. C* **79** (2019) 388, arXiv:1901.07979 [nucl-ex].
- [60] ALICE Collaboration, S. Acharya *et al.*, “Measurement of prompt D⁰, D⁺, D^{*+}, and D_s⁺ production in p-Pb collisions at $\sqrt{s_{NN}} = 5.02$ TeV”, *JHEP* **12** (2019) 092, arXiv:1906.03425 [nucl-ex].
- [61] ALICE Collaboration, S. Acharya *et al.*, “Azimuthal correlations of prompt D mesons with charged particles in pp and p-Pb collisions at $\sqrt{s_{NN}} = 5.02$ TeV”, *Eur. Phys. J. C* **80** (2020) 979, arXiv:1910.14403 [nucl-ex].

- [62] M. Cacciari, G. P. Salam, and G. Soyez, “FastJet User Manual”, *Eur. Phys. J. C* **72** (2012) 1896, arXiv:1111.6097 [hep-ph].
- [63] P. Nason, “A New method for combining NLO QCD with shower Monte Carlo algorithms”, *JHEP* **11** (2004) 040, arXiv:hep-ph/0409146.
- [64] S. Alioli, K. Hamilton, P. Nason, C. Oleari, and E. Re, “Jet pair production in POWHEG”, *JHEP* **04** (2011) 081, arXiv:1012.3380 [hep-ph].
- [65] H.-L. Lai, M. Guzzi, J. Huston, Z. Li, P. M. Nadolsky, J. Pumplin, and C. P. Yuan, “New parton distributions for collider physics”, *Phys. Rev. D* **82** (2010) 074024, arXiv:1007.2241 [hep-ph].
- [66] A. Buckley, J. Ferrando, S. Lloyd, *et al.*, “LHAPDF6: parton density access in the LHC precision era”, *Eur. Phys. J. C* **75** (2015) 132, arXiv:1412.7420 [hep-ph].
- [67] G. D’Agostini, “Improved iterative Bayesian unfolding”, arXiv:1010.0632 [physics.data-an].
- [68] T. Auye, “RooUnfold, a framework for unfolding within the ROOT environment”, Jan., 2021. <https://gitlab.cern.ch/RooUnfold/RooUnfold>.
- [69] ALICE Collaboration, S. Acharya *et al.*, “Measurement of charged jet cross section in pp collisions at $\sqrt{s} = 5.02$ TeV”, *Phys. Rev. D* **100** (2019) 092004, arXiv:1905.02536 [nucl-ex].
- [70] T. Sjöstrand, S. Ask, J. R. Christiansen, *et al.*, “An introduction to PYTHIA 8.2”, *Comput. Phys. Commun.* **191** (2015) 159–177, arXiv:1410.3012 [hep-ph].
- [71] B. Andersson, G. Gustafson, G. Ingelman, and T. Sjostrand, “Parton Fragmentation and String Dynamics”, *Phys. Rept.* **97** (1983) 31–145.
- [72] T. Sjostrand, “Jet Fragmentation of Nearby Partons”, *Nucl. Phys. B* **248** (1984) 469–502.
- [73] J. R. Christiansen and P. Z. Skands, “String Formation Beyond Leading Colour”, *JHEP* **08** (2015) 003, arXiv:1505.01681 [hep-ph].
- [74] S. Frixione, P. Nason, and G. Ridolfi, “A Positive-weight next-to-leading-order Monte Carlo for heavy flavour hadroproduction”, *JHEP* **09** (2007) 126, arXiv:0707.3088 [hep-ph].

A Measurements of D⁰ jets with $R = 0.3$ in pp collisions at $\sqrt{s} = 5.02$ TeV

The $p_{T,\text{chjet}}$ -differential cross section of D⁰ jets with $R = 0.3$ in pp collisions at $\sqrt{s} = 5.02$ TeV compared to PYTHIA 8 and POWHEG+PYTHIA 8 predictions is shown in Fig. A.1. The D⁰-jet fraction of inclusive jets for the same R is shown in Fig. A.2. Fig. A.3 shows the $z_{\parallel}^{\text{ch}}$ distributions for $R = 0.3$ D⁰ jets in four different intervals of $p_{T,\text{chjet}}$ for $\sqrt{s} = 5.02$ TeV.

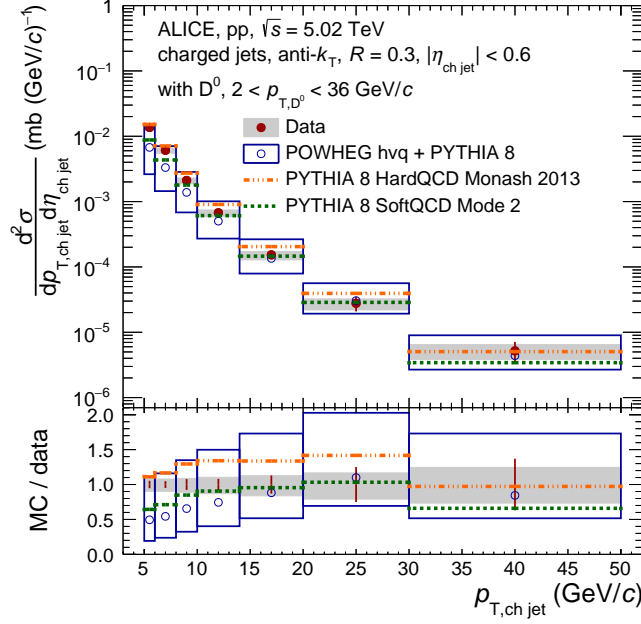


Figure A.1: Top panel: $p_{T,\text{chjet}}$ -differential cross section of charm jets tagged with D⁰ mesons for $R = 0.3$ in pp collisions at $\sqrt{s} = 5.02$ TeV compared to PYTHIA 8 HardQCD Monash 2013 (dash-dotted lines), PYTHIA 8 Monash 2013 SoftQCD Mode 2 (dashed lines) and POWHEG hvq + PYTHIA 8 (open circles) predictions. The shaded bands indicate the systematic uncertainty on the data cross section while open boxes represent the theoretical uncertainties on the POWHEG predictions. Bottom panel presents ratios of MC predictions to the data.

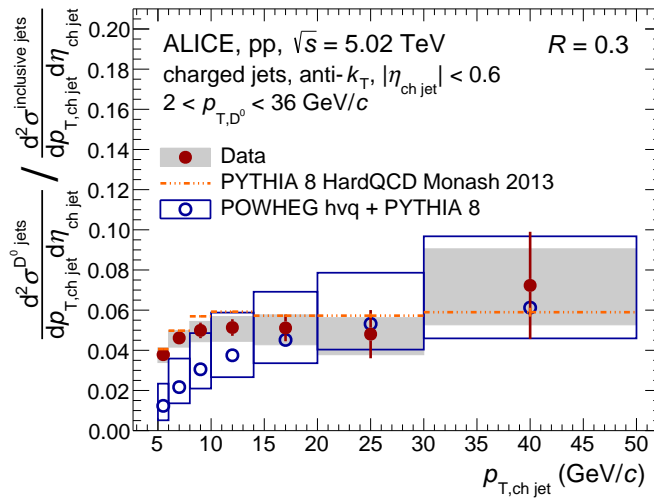


Figure A.2: The fraction of D⁰ jets over inclusive charged-particle jets in pp collisions at $\sqrt{s} = 5.02$ TeV for $R = 0.3$ compared to PYTHIA 8 HardQCD Monash 2013 (dash-dotted lines) and POWHEG hvq + PYTHIA 8 (open circles) predictions.

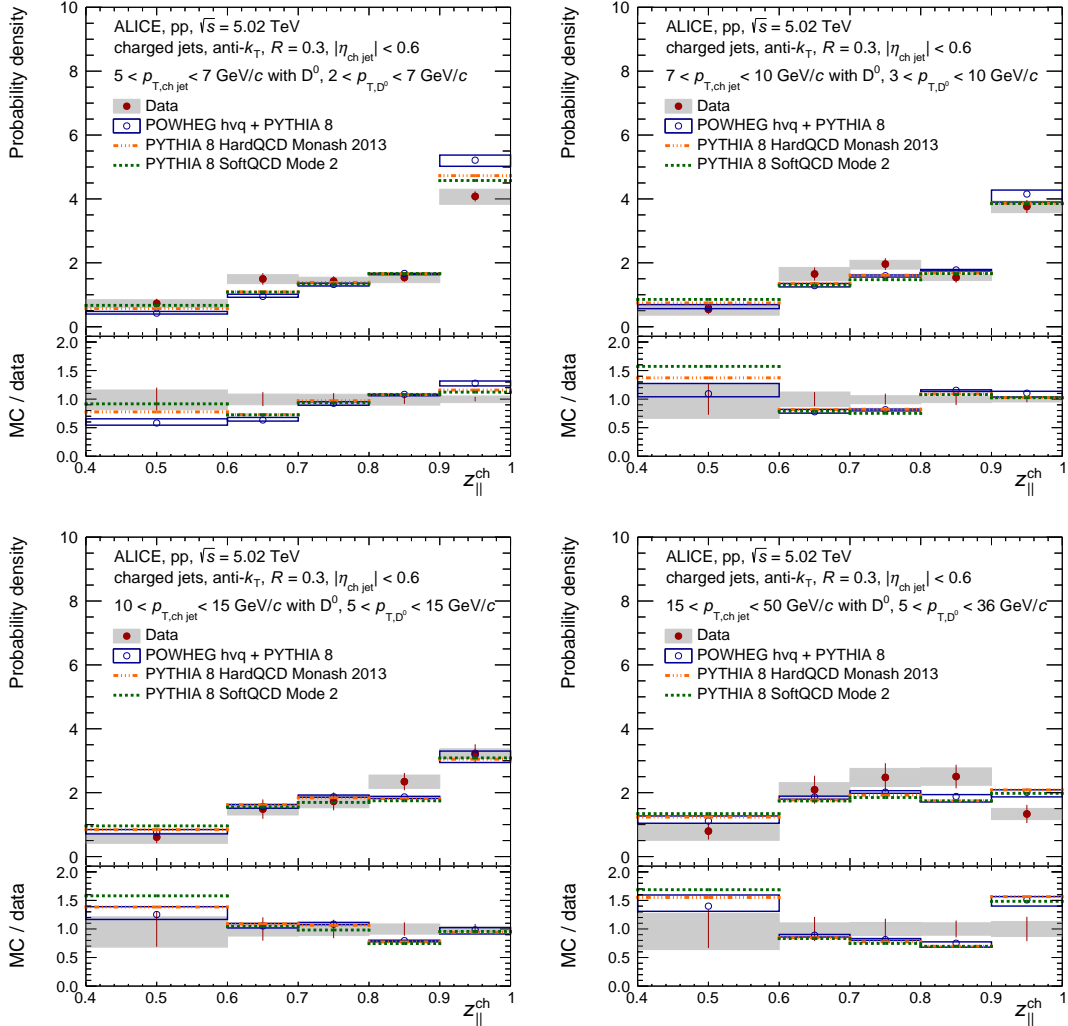


Figure A.3: Top panels: $z_{\parallel}^{\text{ch}}$ -differential yield of $R = 0.3$ charm jets tagged with D^0 mesons normalised by the number of D^0 jets within each distribution in pp collisions at $\sqrt{s} = 5.02$ TeV in four $p_{T, \text{chjet}}$ intervals (top left) $5 < p_{T, \text{chjet}} < 7$ GeV/ c , (top right) $7 < p_{T, \text{chjet}} < 10$ GeV/ c , (bottom left) $10 < p_{T, \text{chjet}} < 15$ GeV/ c and (bottom right) $15 < p_{T, \text{chjet}} < 50$ GeV/ c GeV/ c . They are compared to PYTHIA 8 Monash 2013 (dashed-dotted lines), PYTHIA 8 Monash 2013 SoftQCD Mode 2 (dashed lines) and POWHEG hvq + PYTHIA 8 (open circles) predictions. The shaded bands indicate the systematic uncertainty on the distributions while open boxes represent the theoretical uncertainties on the POWHEG predictions. Bottom panels present ratios of MC predictions to the data.

B The ALICE Collaboration

S. Acharya ^{124,131}, D. Adamová ⁸⁶, A. Adler⁶⁹, G. Aglieri Rinella ³², M. Agnello ²⁹, N. Agrawal ⁵⁰, Z. Ahammed ¹³¹, S. Ahmad ¹⁵, S.U. Ahn ⁷⁰, I. Ahuja ³⁷, A. Akindinov ¹³⁹, M. Al-Turany ⁹⁸, D. Aleksandrov ¹³⁹, B. Alessandro ⁵⁵, H.M. Alfanda ⁶, R. Alfaro Molina ⁶⁶, B. Ali ¹⁵, Y. Ali¹³, A. Alici ²⁵, N. Alizadehvandchali ¹¹³, A. Alkin ³², J. Alme ²⁰, G. Alocco ⁵¹, T. Alt ⁶³, I. Altsybeev ¹³⁹, M.N. Anaam ⁶, C. Andrei ⁴⁵, A. Andronic ¹³⁴, V. Angelov ⁹⁵, F. Antinori ⁵³, P. Antonioli ⁵⁰, C. Anuj ¹⁵, N. Apadula ⁷⁴, L. Aphecetche ¹⁰³, H. Appelshäuser ⁶³, S. Arcelli ²⁵, R. Arnaldi ⁵⁵, I.C. Arsene ¹⁹, M. Arslanok ¹³⁶, A. Augustinus ³², R. Averbeck ⁹⁸, S. Aziz ⁷², M.D. Azmi ¹⁵, A. Badalà ⁵², Y.W. Baek ⁴⁰, X. Bai ⁹⁸, R. Bailhache ⁶³, Y. Bailung ⁴⁷, R. Bala ⁹¹, A. Balbino ²⁹, A. Baldisseri ¹²⁷, B. Balis ², D. Banerjee ⁴, Z. Banoo ⁹¹, R. Barbera ²⁶, L. Barioglio ⁹⁶, M. Barlou⁷⁸, G.G. Barnaföldi ¹³⁵, L.S. Barnby ⁸⁵, V. Barret ¹²⁴, L. Barreto ¹⁰⁹, C. Bartels ¹¹⁶, K. Barth ³², E. Bartsch ⁶³, F. Baruffaldi ²⁷, N. Bastid ¹²⁴, S. Basu ⁷⁵, G. Batigne ¹⁰³, D. Battistini ⁹⁶, B. Batyunya ¹⁴⁰, D. Bauri⁴⁶, J.L. Bazo Alba ¹⁰¹, I.G. Bearden ⁸³, C. Beattie ¹³⁶, P. Becht ⁹⁸, D. Behera ⁴⁷, I. Belikov ¹²⁶, A.D.C. Bell Hechavarria ¹³⁴, F. Bellini ²⁵, R. Bellwied ¹¹³, S. Belokurova ¹³⁹, V. Belyaev ¹³⁹, G. Bencedi ^{135,64}, S. Beole ²⁴, A. Bercuci ⁴⁵, Y. Berdnikov ¹³⁹, A. Berdnikova ⁹⁵, L. Bergmann ⁹⁵, M.G. Besoiu ⁶², L. Betev ³², P.P. Bhaduri ¹³¹, A. Bhasin ⁹¹, I.R. Bhat⁹¹, M.A. Bhat ⁴, B. Bhattacharjee ⁴¹, L. Bianchi ²⁴, N. Bianchi ⁴⁸, J. Bielčik ³⁵, J. Bielčíková ⁸⁶, J. Biernat ¹⁰⁶, A. Bilandzic ⁹⁶, G. Biro ¹³⁵, S. Biswas ⁴, J.T. Blair ¹⁰⁷, D. Blau ¹³⁹, M.B. Blidaru ⁹⁸, N. Bluhme³⁸, C. Blume ⁶³, G. Boca ^{21,54}, F. Bock ⁸⁷, T. Bodova ²⁰, A. Bogdanov¹³⁹, S. Boi ²², J. Bok ⁵⁷, L. Boldizsár ¹³⁵, A. Bolozdynya ¹³⁹, M. Bombara ³⁷, P.M. Bond ³², G. Bonomi ^{130,54}, H. Borel ¹²⁷, A. Borissov ¹³⁹, H. Bossi ¹³⁶, E. Botta ²⁴, L. Bratrud ⁶³, P. Braun-Munzinger ⁹⁸, M. Bregant ¹⁰⁹, M. Broz ³⁵, G.E. Bruno ^{97,31}, M.D. Buckland ¹¹⁶, D. Budnikov ¹³⁹, H. Buesching ⁶³, S. Bufalino ²⁹, O. Bugnon¹⁰³, P. Buhler ¹⁰², Z. Buthelezi ^{67,120}, J.B. Butt¹³, A. Bylinkin ¹¹⁵, S.A. Bysiak¹⁰⁶, M. Cai ^{27,6}, H. Caines ¹³⁶, A. Caliva ⁹⁸, E. Calvo Villar ¹⁰¹, J.M.M. Camacho ¹⁰⁸, R.S. Camacho⁴⁴, P. Camerini ²³, F.D.M. Canedo ¹⁰⁹, M. Carabas ¹²³, F. Carnesecchi ³², R. Caron ^{125,127}, J. Castillo Castellanos ¹²⁷, F. Catalano ²⁹, C. Ceballos Sanchez ¹⁴⁰, I. Chakaberia ⁷⁴, P. Chakraborty ⁴⁶, S. Chandra ¹³¹, S. Chapeland ³², M. Chartier ¹¹⁶, S. Chattopadhyay ¹³¹, S. Chattopadhyay ⁹⁹, T.G. Chavez ⁴⁴, T. Cheng ⁶, C. Cheshkov ¹²⁵, B. Cheynis ¹²⁵, V. Chibante Barroso ³², D.D. Chinellato ¹¹⁰, E.S. Chizzali ^{11,96}, J. Cho ⁵⁷, S. Cho ⁵⁷, P. Chochula ³², P. Christakoglou ⁸⁴, C.H. Christensen ⁸³, P. Christiansen ⁷⁵, T. Chujo ¹²², M. Ciaccio ²⁹, C. Cicalo ⁵¹, L. Cifarelli ²⁵, F. Cindolo ⁵⁰, M.R. Ciupek⁹⁸, G. Clai^{III,50}, F. Colamaria ⁴⁹, J.S. Colburn¹⁰⁰, D. Colella ^{97,31}, A. Collu⁷⁴, M. Colocci ³², M. Concas ^{IV,55}, G. Conesa Balbastre ⁷³, Z. Conesa del Valle ⁷², G. Contin ²³, J.G. Contreras ³⁵, M.L. Coquet ¹²⁷, T.M. Cormier^{I,87}, P. Cortese ^{129,55}, M.R. Cosentino ¹¹¹, F. Costa ³², S. Costanza ^{21,54}, P. Crochet ¹²⁴, R. Cruz-Torres ⁷⁴, E. Cuautele⁶⁴, P. Cui ⁶, L. Cunqueiro⁸⁷, A. Dainese ⁵³, M.C. Danisch ⁹⁵, A. Danu ⁶², P. Das ⁸⁰, P. Das ⁴, S. Das ⁴, S. Dash ⁴⁶, A. De Caro ²⁸, G. de Cataldo ⁴⁹, L. De Cilladi ²⁴, J. de Cuveland³⁸, A. De Falco ²², D. De Gruttola ²⁸, N. De Marco ⁵⁵, C. De Martin ²³, S. De Pasquale ²⁸, S. Deb ⁴⁷, H.F. Degenhardt¹⁰⁹, K.R. Deja ¹³², R. Del Grande ⁹⁶, L. Dello Stritto ²⁸, W. Deng ⁶, P. Dhankher ¹⁸, D. Di Bari ³¹, A. Di Mauro ³², R.A. Diaz ^{140,7}, T. Dietel ¹¹², Y. Ding ^{125,6}, R. Divià ¹⁸, D.U. Dixit ¹⁸, Ø. Djuvsland²⁰, U. Dmitrieva ¹³⁹, A. Dobrin ⁶², B. Dönigus ⁶³, A.K. Dubey ¹³¹, J.M. Dubinski¹³², A. Dubla ⁹⁸, S. Dudi ⁹⁰, P. Dupieux ¹²⁴, M. Durkac¹⁰⁵, N. Dzalaiova¹², T.M. Eder ¹³⁴, R.J. Ehlers ⁸⁷, V.N. Eikeland²⁰, F. Eisenhut ⁶³, D. Elia ⁴⁹, B. Erasmus ¹⁰³, F. Ercolessi ²⁵, F. Erhardt ⁸⁹, M.R. Ersdal²⁰, B. Espagnon ⁷², G. Eulisse ³², D. Evans ¹⁰⁰, S. Evdokimov ¹³⁹, L. Fabbietti ⁹⁶, M. Faggin ²⁷, J. Faivre ²⁷, F. Fan ⁶, W. Fan ⁷⁴, A. Fantoni ⁴⁸, M. Fasel ⁸⁷, P. Fecchio²⁹, A. Feliciello ⁵⁵, G. Feofilov ¹³⁹, A. Fernández Téllez ⁴⁴, M.B. Ferrer ³², A. Ferrero ¹²⁷, A. Ferretti ²⁴, V.J.G. Feuillard ⁹⁵, J. Figiel ¹⁰⁶, V. Filova³⁵, D. Finogeev ¹³⁹, F.M. Fionda ⁵¹, G. Fiorenza⁹⁷, F. Flor ¹¹³, A.N. Flores ¹⁰⁷, S. Foertsch ⁶⁷, I. Fokin ⁹⁵, S. Fokin ¹³⁹, E. Fragiaco ⁵⁶, E. Frajna ¹³⁵, U. Fuchs ³², N. Funicello ²⁸, C. Furget ⁷³, A. Furs ¹³⁹, J.J. Gaardhøje ⁸³, M. Gagliardi ²⁴, A.M. Gago ¹⁰¹, A. Gal¹²⁶, C.D. Galvan ¹⁰⁸, P. Ganoti ⁷⁸, C. Garabatos ⁹⁸, J.R.A. García ⁴⁴, E. García-Solis ⁹, K. Garg ¹⁰³, C. Gargiulo ³², A. Garibli⁸¹, K. Garner¹³⁴, E.F. Gauger ¹⁰⁷, A. Gautam ¹¹⁵, M.B. Gay Ducati ⁶⁵, M. Germain ¹⁰³, S.K. Ghosh⁴, M. Giacalone ²⁵, P. Gianotti ⁴⁸, P. Giubellino ^{98,55}, P. Giubilato ²⁷, A.M.C. Glaenger ¹²⁷, P. Glässel ⁹⁵, E. Glimos¹¹⁹, D.J.Q. Goh⁷⁶, V. Gonzalez ¹³³, L.H. González-Trueba ⁶⁶, S. Gorbunov³⁸, M. Gorgon ², L. Görlich ¹⁰⁶, S. Gotovac³³, V. Grabski ⁶⁶, L.K. Graczykowski ¹³², E. Grecka ⁸⁶, L. Greiner ⁷⁴, A. Grelli ⁵⁸, C. Grigoras ³², V. Grigoriev ¹³⁹, S. Grigoryan ^{140,1}, F. Grosa ³², J.F. Grosse-Oetringhaus ³², R. Grosso ⁹⁸, D. Grund ³⁵, G.G. Guardianio ¹¹⁰, R. Guernane ⁷³, M. Guilbaud ¹⁰³, K. Gulbrandsen ⁸³, T. Gunji ¹²¹, W. Guo ⁶, A. Gupta ⁹¹, R. Gupta ⁹¹,

S.P. Guzman⁴⁴, L. Gyulai¹³⁵, M.K. Habib⁹⁸, C. Hadjidakis⁷², H. Hamagaki⁷⁶, M. Hamid⁶, Y. Han¹³⁷, R. Hannigan¹⁰⁷, M.R. Haque¹³², A. Harlenderova⁹⁸, J.W. Harris¹³⁶, A. Harton⁹, J.A. Hasenbichler³², H. Hassan⁸⁷, D. Hatzifotiadou⁵⁰, P. Hauer⁴², L.B. Havener¹³⁶, S.T. Heckel⁹⁶, E. Hellbär⁹⁸, H. Helstrup³⁴, T. Herman³⁵, G. Herrera Corral⁸, F. Herrmann¹³⁴, K.F. Hetland³⁴, B. Heybeck⁶³, H. Hillemanns³², C. Hills¹¹⁶, B. Hippolyte¹²⁶, B. Hofman⁵⁸, B. Hohlweger⁸⁴, J. Honeremann¹³⁴, G.H. Hong¹³⁷, D. Horak³⁵, A. Horzyk², R. Hosokawa¹⁴, Y. Hou⁶, P. Hristov³², C. Hughes¹¹⁹, P. Huhn⁶³, L.M. Huhta¹¹⁴, C.V. Hulse⁷², T.J. Humanic⁸⁸, H. Hushnud⁹⁹, A. Hutson¹¹³, D. Hutter³⁸, J.P. Iddon¹¹⁶, R. Ilkaev¹³⁹, H. Ilyas¹³, M. Inaba¹²², G.M. Innocenti³², M. Ippolitov¹³⁹, A. Isakov⁸⁶, T. Isidori¹¹⁵, M.S. Islam⁹⁹, M. Ivanov⁹⁸, V. Ivanov¹³⁹, V. Izucheev¹³⁹, M. Jablonski², B. Jacak⁷⁴, N. Jacazio³², P.M. Jacobs⁷⁴, S. Jadlovská¹⁰⁵, J. Jadlovsky¹⁰⁵, L. Jaffe³⁸, C. Jahnke¹¹⁰, M.A. Janik¹³², T. Janson⁶⁹, M. Jercic⁸⁹, O. Jevons¹⁰⁰, A.A.P. Jimenez⁶⁴, F. Jonas^{87,134}, P.G. Jones¹⁰⁰, J.M. Jowett^{32,98}, J. Jung⁶³, M. Jung⁶³, A. Junique³², A. Jusko¹⁰⁰, M.J. Kabus^{32,132}, J. Kaewjai¹⁰⁴, P. Kalinak⁵⁹, A.S. Kalteyer⁹⁸, A. Kalweit³², V. Kaplin¹³⁹, A. Karasu Uysal⁷¹, D. Karatovic⁸⁹, O. Karavichev¹³⁹, T. Karavicheva¹³⁹, P. Karczmarczyk¹³², E. Karpechev¹³⁹, V. Kashyap⁸⁰, A. Kazantsev¹³⁹, U. Keschull⁶⁹, R. Keidel¹³⁸, D.L.D. Keijdener⁵⁸, M. Keil³², B. Ketzer⁴², A.M. Khan⁶, S. Khan¹⁵, A. Khanzadeev¹³⁹, Y. Kharlov¹³⁹, A. Khatun¹⁵, A. Khuntia¹⁰⁶, B. Kileng³⁴, B. Kim¹⁶, C. Kim¹⁶, D.J. Kim¹¹⁴, E.J. Kim⁶⁸, J. Kim¹³⁷, J.S. Kim⁴⁰, J. Kim⁹⁵, J. Kim⁶⁸, M. Kim⁹⁵, S. Kim¹⁷, T. Kim¹³⁷, S. Kirsch⁶³, I. Kisel³⁸, S. Kiselev¹³⁹, A. Kisiel¹³², J.P. Kitowski², J.L. Klay⁵, J. Klein³², S. Klein⁷⁴, C. Klein-Bösing¹³⁴, M. Kleiner⁶³, T. Klemenz⁹⁶, A. Kluge³², A.G. Knospe¹¹³, C. Kobdaj¹⁰⁴, T. Kollegger⁹⁸, A. Kondratyev¹⁴⁰, N. Kondratyeva¹³⁹, E. Kondratyuk¹³⁹, J. Konig⁶³, S.A. Konigstorfer⁹⁶, P.J. Konopka³², G. Kornakov¹³², S.D. Koryciak², A. Kotliarov⁸⁶, O. Kovalenko⁷⁹, V. Kovalenko¹³⁹, M. Kowalski¹⁰⁶, I. Králik⁵⁹, A. Kravčáková³⁷, L. Kreis⁹⁸, M. Krivda^{100,59}, F. Krizek⁸⁶, K. Krizkova Gajdosova³⁵, M. Kroesen⁹⁵, M. Krüger⁶³, D.M. Krupova³⁵, E. Kryshen¹³⁹, M. Krzewicki³⁸, V. Kučera³², C. Kuhn¹²⁶, P.G. Kuijer⁸⁴, T. Kumaoka¹²², D. Kumar¹³¹, L. Kumar⁹⁰, N. Kumar⁹⁰, S. Kundu³², P. Kurashvili⁷⁹, A. Kurepin¹³⁹, A.B. Kurepin¹³⁹, S. Kushpil⁸⁶, J. Kvapil¹⁰⁰, M.J. Kweon⁵⁷, J.Y. Kwon⁵⁷, Y. Kwon¹³⁷, S.L. La Pointe³⁸, P. La Rocca²⁶, Y.S. Lai⁷⁴, A. Lakrathok¹⁰⁴, M. Lamanna³², R. Langoy¹¹⁸, P. Larionov⁴⁸, E. Laudi³², L. Lautner^{32,96}, R. Lavicka¹⁰², T. Lazareva¹³⁹, R. Lea^{130,54}, J. Leibrach³⁸, R.C. Lemmon⁸⁵, I. León Monzón¹⁰⁸, M.M. Lesch⁹⁶, E.D. Lesser¹⁸, M. Lettrich⁹⁶, P. Lévai¹³⁵, X. Li¹⁰, X.L. Li⁶, J. Lien¹¹⁸, R. Lietava¹⁰⁰, B. Lim¹⁶, S.H. Lim¹⁶, V. Lindenstruth³⁸, A. Lindner⁴⁵, C. Lippmann⁹⁸, A. Liu¹⁸, D.H. Liu⁶, J. Liu¹¹⁶, I.M. Lofnes²⁰, V. Loginov¹³⁹, C. Loizides⁸⁷, P. Loncar³³, J.A. Lopez⁹⁵, X. Lopez¹²⁴, E. López Torres⁷, P. Lu^{98,117}, J.R. Luhder¹³⁴, M. Lunardon²⁷, G. Luparello⁵⁶, Y.G. Ma³⁹, A. Maevskaya¹³⁹, M. Mager³², T. Mahmoud⁴², A. Maire¹²⁶, M. Malaev¹³⁹, N.M. Malik⁹¹, Q.W. Malik¹⁹, S.K. Malik⁹¹, L. Malinina^{VII,140}, D. Mal'Kevich¹³⁹, D. Mallick⁸⁰, N. Mallick⁴⁷, G. Mandaglio^{30,52}, V. Manko¹³⁹, F. Manso¹²⁴, V. Manzari⁴⁹, Y. Mao⁶, G.V. Margagliotti²³, A. Margotti⁵⁰, A. Marín⁹⁸, C. Markert¹⁰⁷, M. Marquard⁶³, N.A. Martin⁹⁵, P. Martinengo³², J.L. Martinez¹¹³, M.I. Martínez⁴⁴, G. Martínez García¹⁰³, S. Masciocchi⁹⁸, M. Masera²⁴, A. Masoni⁵¹, L. Massacrier⁷², A. Mastroserio^{128,49}, A.M. Mathis⁹⁶, O. Matonoha⁷⁵, P.F.T. Matuoka¹⁰⁹, A. Matyja¹⁰⁶, C. Mayer¹⁰⁶, A.L. Mazuecos³², F. Mazzaschi²⁴, M. Mazzilli³², J.E. Mdhuli¹²⁰, A.F. Mechler⁶³, Y. Melikyan¹³⁹, A. Menchaca-Rocha⁶⁶, E. Meninno^{102,28}, A.S. Menon¹¹³, M. Meres¹², S. Mhlanga^{112,67}, Y. Miake¹²², L. Micheletti⁵⁵, L.C. Migliorin¹²⁵, D.L. Mihaylov⁹⁶, K. Mikhaylov^{140,139}, A. Mischke^{I,58}, A.N. Mishra¹³⁵, D. Miśkowiec⁹⁸, A. Modak⁴, A.P. Mohanty⁵⁸, B. Mohanty⁸⁰, M. Mohisin Khan^{V,15}, M.A. Molander⁴³, Z. Moravcova⁸³, C. Mordasini⁹⁶, D.A. Moreira De Godoy¹³⁴, I. Morozov¹³⁹, A. Morsch³², T. Mrnjavac³², V. Muccifora⁴⁸, E. Mudnic³³, S. Muhuri¹³¹, J.D. Mulligan⁷⁴, A. Mulliri²², M.G. Munhoz¹⁰⁹, R.H. Munzer⁶³, H. Murakami¹²¹, S. Murray¹¹², L. Musa³², J. Musinsky⁵⁹, J.W. Myrcha¹³², B. Naik¹²⁰, R. Nair⁷⁹, B.K. Nandi⁴⁶, R. Nania⁵⁰, E. Nappi⁴⁹, A.F. Nassirpour⁷⁵, A. Nath⁹⁵, C. Nattrass¹¹⁹, A. Neagu¹⁹, A. Negru¹²³, L. Nellen⁶⁴, S.V. Nesbo³⁴, G. Neskovic³⁸, D. Nesterov¹³⁹, B.S. Nielsen⁸³, E.G. Nielsen⁸³, S. Nikolaev¹³⁹, S. Nikulin¹³⁹, V. Nikulin¹³⁹, F. Noferini⁵⁰, S. Noh¹¹, P. Nomokonov¹⁴⁰, J. Norman¹¹⁶, N. Novitzky¹²², P. Nowakowski¹³², A. Nyanin¹³⁹, J. Nystrand²⁰, M. Ogino⁷⁶, A. Ohlson⁷⁵, V.A. Okorokov¹³⁹, J. Oleniacz¹³², A.C. Oliveira Da Silva¹¹⁹, M.H. Oliver¹³⁶, A. Onnerstad¹¹⁴, C. Oppedisano⁵⁵, A. Ortiz Velasquez⁶⁴, A. Oskarsson⁷⁵, J. Otwinowski¹⁰⁶, M. Oya⁹³, K. Oyama⁷⁶, Y. Pachmayer⁹⁵, S. Padhan⁴⁶, D. Pagano^{130,54}, G. Paić⁶⁴, A. Palasciano⁴⁹, S. Panebianco¹²⁷, J. Park⁵⁷, J.E. Parkkila^{32,114}, S.P. Pathak¹¹³, R.N. Patra⁹¹, B. Paul²², H. Pei⁶, T. Peitzmann⁵⁸, X. Peng⁶, L.G. Pereira⁶⁵, H. Pereira Da Costa¹²⁷, D. Peresunko¹³⁹, G.M. Perez⁷, S. Perrin¹²⁷,

Y. Pestov¹³⁹, V. Petráček³⁵, V. Petrov¹³⁹, M. Petrovici⁴⁵, R.P. Pezzi^{103,65}, S. Piano⁵⁶, M. Pikna¹², P. Pillot¹⁰³, O. Pinazza^{50,32}, L. Pinsky¹¹³, C. Pinto^{96,26}, S. Pisano⁴⁸, M. Płoskoń⁷⁴, M. Planinic⁸⁹, F. Pliquett⁶³, M.G. Poghosyan⁸⁷, S. Politano²⁹, N. Poljak⁸⁹, A. Pop⁴⁵, S. Porteboeuf-Houssais¹²⁴, J. Porter⁷⁴, V. Pozdniakov¹⁴⁰, S.K. Prasad⁴, S. Prasad⁴⁷, R. Preghenella⁵⁰, F. Prino⁵⁵, C.A. Pruneau¹³³, I. Pshenichnov¹³⁹, M. Puccio³², S. Qiu⁸⁴, L. Quaglia²⁴, R.E. Quishpe¹¹³, S. Ragoni¹⁰⁰, A. Rakotozafindrabe¹²⁷, L. Ramello^{129,55}, F. Rami¹²⁶, S.A.R. Ramirez⁴⁴, T.A. Rancien⁷³, R. Raniwala⁹², S. Raniwala⁹², S.S. Räsänen⁴³, R. Rath⁴⁷, I. Ravasenga⁸⁴, K.F. Read^{87,119}, A.R. Redelbach³⁸, K. Redlich^{VI,79}, A. Rehman²⁰, P. Reichelt⁶³, F. Reidt³², H.A. Reme-Ness³⁴, Z. Rescakova³⁷, K. Reygers⁹⁵, A. Riabov¹³⁹, V. Riabov¹³⁹, R. Ricci²⁸, T. Richert⁷⁵, M. Richter¹⁹, W. Riegler³², F. Riggi²⁶, C. Ristea⁶², M. Rodríguez Cahuantzi⁴⁴, K. Røed¹⁹, R. Rogalev¹³⁹, E. Rogochaya¹⁴⁰, T.S. Rogoschinski⁶³, D. Rohr³², D. Röhrich²⁰, P.F. Rojas⁴⁴, S. Rojas Torres³⁵, P.S. Rokita¹³², F. Ronchetti⁴⁸, A. Rosano^{30,52}, E.D. Rosas⁶⁴, A. Rossi⁵³, A. Roy⁴⁷, P. Roy⁹⁹, S. Roy⁴⁶, N. Rubini²⁵, O.V. Rueda⁷⁵, D. Ruggiano¹³², R. Rui²³, B. Rumyantsev¹⁴⁰, P.G. Russek², R. Russo⁸⁴, A. Rustamov⁸¹, E. Ryabinkin¹³⁹, Y. Ryabov¹³⁹, A. Rybicki¹⁰⁶, H. Rytönen¹¹⁴, W. Rzesza¹³², O.A.M. Saarimäki⁴³, R. Sadek¹⁰³, S. Sadovsky¹³⁹, J. Saetre²⁰, K. Šafařík³⁵, S.K. Saha¹³¹, S. Saha⁸⁰, B. Sahoo⁴⁶, P. Sahoo⁴⁶, R. Sahoo⁴⁷, S. Sahoo⁶⁰, D. Sahu⁴⁷, P.K. Sahu⁶⁰, J. Saini¹³¹, K. Sajdakova³⁷, S. Sakai¹²², M.P. Salvan⁹⁸, S. Sambyal⁹¹, T.B. Saramela¹⁰⁹, D. Sarkar¹³³, N. Sarkar¹³¹, P. Sarma⁴¹, V. Sarritzu²², V.M. Sarti⁹⁶, M.H.P. Sas¹³⁶, J. Schambach⁸⁷, H.S. Scheid⁶³, C. Schiaua⁴⁵, R. Schicker⁹⁵, A. Schmah⁹⁵, C. Schmidt⁹⁸, H.R. Schmidt⁹⁴, M.O. Schmidt³², M. Schmidt⁹⁴, N.V. Schmidt^{87,63}, A.R. Schmier¹¹⁹, R. Schotter¹²⁶, J. Schukraft³², K. Schwarz⁹⁸, K. Schweda⁹⁸, G. Scioli²⁵, E. Scapparini⁵⁵, J.E. Seger¹⁴, Y. Sekiguchi¹²¹, D. Sekihata¹²¹, I. Selyuzhenkov^{98,139}, S. Senyukov¹²⁶, J.J. Seo⁵⁷, D. Serebryakov¹³⁹, L. Šerkšnytė⁹⁶, A. Sevcenco⁶², T.J. Shaba⁶⁷, A. Shabanov¹³⁹, A. Shabetai¹⁰³, R. Shahoyan³², W. Shaikh⁹⁹, A. Shangaraev¹³⁹, A. Sharma⁹⁰, D. Sharma⁴⁶, H. Sharma¹⁰⁶, M. Sharma⁹¹, N. Sharma⁹⁰, S. Sharma⁹¹, U. Sharma⁹¹, A. Shatat⁷², O. Sheibani¹¹³, K. Shigaki⁹³, M. Shimomura⁷⁷, S. Shirinkin¹³⁹, Q. Shou³⁹, Y. Sibiriak¹³⁹, S. Siddhanta⁵¹, T. Siemiarczuk⁷⁹, T.F. Silva¹⁰⁹, D. Silvermyr⁷⁵, T. Simantathammakul¹⁰⁴, R. Simeonov³⁶, G. Simonetti³², B. Singh⁹¹, B. Singh⁹⁶, R. Singh⁸⁰, R. Singh⁹¹, R. Singh⁴⁷, V.K. Singh¹³¹, V. Singhal¹³¹, T. Sinha⁹⁹, B. Sitar¹², M. Sitta^{129,55}, T.B. Skaali¹⁹, G. Skorodumovs⁹⁵, M. Slupecki⁴³, N. Smirnov¹³⁶, R.J.M. Snellings⁵⁸, E.H. Solheim¹⁹, C. Soncco¹⁰¹, J. Song¹¹³, A. Songmoolnak¹⁰⁴, F. Soramel²⁷, S. Sorensen¹¹⁹, R. Spijkers⁸⁴, I. Sputowska¹⁰⁶, J. Staa⁷⁵, J. Stachel⁹⁵, I. Stan⁶², P.J. Steffanic¹¹⁹, S.F. Stiefelmaier⁹⁵, D. Stocco¹⁰³, I. Storehaug¹⁹, M.M. Storetvedt³⁴, P. Stratmann¹³⁴, S. Strazzi²⁵, C.P. Stylianidis⁸⁴, A.A.P. Suaide¹⁰⁹, C. Suire⁷², M. Sukhanov¹³⁹, M. Suljic³², V. Sumberia⁹¹, S. Sumowidagdo⁸², S. Swain⁶⁰, A. Szabo¹², I. Szarka¹², U. Tabassam¹³, S.F. Taghavi⁹⁶, G. TAILLEPIED^{98,124}, J. Takahashi¹¹⁰, G.J. Tambave²⁰, S. Tang^{124,6}, Z. Tang¹¹⁷, J.D. Tapia Takaki¹¹⁵, N. Tapus¹²³, L.A. Tarasovicova¹³⁴, M.G. Tarzila⁴⁵, A. Tauro³², A. Telesca³², L. Terlizzi²⁴, C. Terrevoli¹¹³, G. Tersimonov³, S. Thakur¹³¹, D. Thomas¹⁰⁷, R. Tieulent¹²⁵, A. Tikhonov¹³⁹, A.R. Timmins¹¹³, M. Tkacik¹⁰⁵, T. Tkacik¹⁰⁵, A. Toia⁶³, N. Topilskaya¹³⁹, M. Toppi⁴⁸, F. Torres-Acosta¹⁸, T. Tork⁷², A.G. Torres Ramos³¹, A. Trifiró^{30,52}, A.S. Triolo^{30,52}, S. Tripathy⁵⁰, T. Tripathy⁴⁶, S. Trogolo³², V. Trubnikov³, W.H. Trzaska¹¹⁴, T.P. Trzcinski¹³², B.A. Trzeciak³⁵, R. Turrisi⁵³, T.S. Tveter¹⁹, K. Ullaland²⁰, B. Ulukutlu⁹⁶, A. Uras¹²⁵, M. Urioni^{54,130}, G.L. Usai²², M. Vala³⁷, N. Valle²¹, S. Vallero⁵⁵, L.V.R. van Doremalen⁵⁸, M. van Leeuwen⁸⁴, C.A. van Veen⁹⁵, R.J.G. van Weelden⁸⁴, P. Vande Vyvre³², D. Varga¹³⁵, Z. Varga¹³⁵, M. Varga-Kofarago¹³⁵, M. Vasileiou⁷⁸, A. Vasiliev¹³⁹, O. Vázquez Doce⁹⁶, V. Vechernin¹³⁹, E. Vercellin²⁴, S. Vergara Limón⁴⁴, L. Vermunt⁵⁸, R. Vértesi¹³⁵, M. Verweij⁵⁸, L. Vickovic³³, Z. Vilakazi¹²⁰, O. Villalobos Baillie¹⁰⁰, G. VINO⁴⁹, A. Vinogradov¹³⁹, T. Virgili²⁸, V. Vislavicius⁸³, A. Vodopyanov¹⁴⁰, B. Volkel³², M.A. Völkl⁹⁵, K. Voloshin¹³⁹, S.A. Voloshin¹³³, G. Volpe³¹, B. von Haller³², I. Vorobyev⁹⁶, N. Vozniuk¹³⁹, J. Vrláková³⁷, B. Wagner²⁰, C. Wang³⁹, D. Wang³⁹, M. Weber¹⁰², A. Wegrzynek³², F.T. Weiglhofer³⁸, S.C. Wenzel³², J.P. Wessels¹³⁴, S.L. Weyhmler¹³⁶, J. Wiechula⁶³, J. Wikne¹⁹, G. Wilk⁷⁹, J. Wilkinson⁹⁸, G.A. Willems¹³⁴, B. Windelband⁹⁵, M. Winn¹²⁷, J.R. Wright¹⁰⁷, W. Wu³⁹, Y. Wu¹¹⁷, R. Xu⁶, A.K. Yadav¹³¹, S. Yalcin⁷¹, Y. Yamaguchi⁹³, K. Yamakawa⁹³, S. Yang²⁰, S. Yano⁹³, Z. Yin⁶, I.-K. Yoo¹⁶, J.H. Yoon⁵⁷, S. Yuan²⁰, A. Yuncu⁹⁵, V. Zaccolo²³, C. Zampolli³², H.J.C. Zanoli⁵⁸, F. Zanone⁹⁵, N. Zardoshti^{32,100}, A. Zarochentsev¹³⁹, P. Závada⁶¹, N. Zaviyalov¹³⁹, M. Zhalov¹³⁹, B. Zhang⁶, S. Zhang³⁹, X. Zhang⁶, Y. Zhang¹¹⁷, M. Zhao¹⁰, V. Zhrebchevskii¹³⁹, Y. Zhi¹⁰, N. Zhigareva¹³⁹, D. Zhou⁶, Y. Zhou⁸³, J. Zhu^{98,6}, Y. Zhu⁶, G. Zinovjev^{I,3}, N. Zurlo^{130,54}

Affiliation Notes

- ^I Deceased
^{II} Also at: Max-Planck-Institut für Physik, Munich, Germany
^{III} Also at: Italian National Agency for New Technologies, Energy and Sustainable Economic Development (ENEA), Bologna, Italy
^{IV} Also at: Dipartimento DET del Politecnico di Torino, Turin, Italy
^V Also at: Department of Applied Physics, Aligarh Muslim University, Aligarh, India
^{VI} Also at: Institute of Theoretical Physics, University of Wrocław, Poland
^{VII} Also at: An institution covered by a cooperation agreement with CERN

Collaboration Institutes

- ¹ A.I. Alikhanyan National Science Laboratory (Yerevan Physics Institute) Foundation, Yerevan, Armenia
² AGH University of Science and Technology, Cracow, Poland
³ Bogolyubov Institute for Theoretical Physics, National Academy of Sciences of Ukraine, Kiev, Ukraine
⁴ Bose Institute, Department of Physics and Centre for Astroparticle Physics and Space Science (CAPSS), Kolkata, India
⁵ California Polytechnic State University, San Luis Obispo, California, United States
⁶ Central China Normal University, Wuhan, China
⁷ Centro de Aplicaciones Tecnológicas y Desarrollo Nuclear (CEADEN), Havana, Cuba
⁸ Centro de Investigación y de Estudios Avanzados (CINVESTAV), Mexico City and Mérida, Mexico
⁹ Chicago State University, Chicago, Illinois, United States
¹⁰ China Institute of Atomic Energy, Beijing, China
¹¹ Chungbuk National University, Cheongju, Republic of Korea
¹² Comenius University Bratislava, Faculty of Mathematics, Physics and Informatics, Bratislava, Slovak Republic
¹³ COMSATS University Islamabad, Islamabad, Pakistan
¹⁴ Creighton University, Omaha, Nebraska, United States
¹⁵ Department of Physics, Aligarh Muslim University, Aligarh, India
¹⁶ Department of Physics, Pusan National University, Pusan, Republic of Korea
¹⁷ Department of Physics, Sejong University, Seoul, Republic of Korea
¹⁸ Department of Physics, University of California, Berkeley, California, United States
¹⁹ Department of Physics, University of Oslo, Oslo, Norway
²⁰ Department of Physics and Technology, University of Bergen, Bergen, Norway
²¹ Dipartimento di Fisica, Università di Pavia, Pavia, Italy
²² Dipartimento di Fisica dell'Università and Sezione INFN, Cagliari, Italy
²³ Dipartimento di Fisica dell'Università and Sezione INFN, Trieste, Italy
²⁴ Dipartimento di Fisica dell'Università and Sezione INFN, Turin, Italy
²⁵ Dipartimento di Fisica e Astronomia dell'Università and Sezione INFN, Bologna, Italy
²⁶ Dipartimento di Fisica e Astronomia dell'Università and Sezione INFN, Catania, Italy
²⁷ Dipartimento di Fisica e Astronomia dell'Università and Sezione INFN, Padova, Italy
²⁸ Dipartimento di Fisica 'E.R. Caianiello' dell'Università and Gruppo Collegato INFN, Salerno, Italy
²⁹ Dipartimento DISAT del Politecnico and Sezione INFN, Turin, Italy
³⁰ Dipartimento di Scienze MIFT, Università di Messina, Messina, Italy
³¹ Dipartimento Interateneo di Fisica 'M. Merlin' and Sezione INFN, Bari, Italy
³² European Organization for Nuclear Research (CERN), Geneva, Switzerland
³³ Faculty of Electrical Engineering, Mechanical Engineering and Naval Architecture, University of Split, Split, Croatia
³⁴ Faculty of Engineering and Science, Western Norway University of Applied Sciences, Bergen, Norway
³⁵ Faculty of Nuclear Sciences and Physical Engineering, Czech Technical University in Prague, Prague, Czech Republic
³⁶ Faculty of Physics, Sofia University, Sofia, Bulgaria
³⁷ Faculty of Science, P.J. Šafárik University, Košice, Slovak Republic
³⁸ Frankfurt Institute for Advanced Studies, Johann Wolfgang Goethe-Universität Frankfurt, Frankfurt, Germany
³⁹ Fudan University, Shanghai, China
⁴⁰ Gangneung-Wonju National University, Gangneung, Republic of Korea
⁴¹ Gauhati University, Department of Physics, Guwahati, India

- 42 Helmholtz-Institut für Strahlen- und Kernphysik, Rheinische Friedrich-Wilhelms-Universität Bonn, Bonn, Germany
- 43 Helsinki Institute of Physics (HIP), Helsinki, Finland
- 44 High Energy Physics Group, Universidad Autónoma de Puebla, Puebla, Mexico
- 45 Horia Hulubei National Institute of Physics and Nuclear Engineering, Bucharest, Romania
- 46 Indian Institute of Technology Bombay (IIT), Mumbai, India
- 47 Indian Institute of Technology Indore, Indore, India
- 48 INFN, Laboratori Nazionali di Frascati, Frascati, Italy
- 49 INFN, Sezione di Bari, Bari, Italy
- 50 INFN, Sezione di Bologna, Bologna, Italy
- 51 INFN, Sezione di Cagliari, Cagliari, Italy
- 52 INFN, Sezione di Catania, Catania, Italy
- 53 INFN, Sezione di Padova, Padova, Italy
- 54 INFN, Sezione di Pavia, Pavia, Italy
- 55 INFN, Sezione di Torino, Turin, Italy
- 56 INFN, Sezione di Trieste, Trieste, Italy
- 57 Inha University, Incheon, Republic of Korea
- 58 Institute for Gravitational and Subatomic Physics (GRASP), Utrecht University/Nikhef, Utrecht, Netherlands
- 59 Institute of Experimental Physics, Slovak Academy of Sciences, Košice, Slovak Republic
- 60 Institute of Physics, Homi Bhabha National Institute, Bhubaneswar, India
- 61 Institute of Physics of the Czech Academy of Sciences, Prague, Czech Republic
- 62 Institute of Space Science (ISS), Bucharest, Romania
- 63 Institut für Kernphysik, Johann Wolfgang Goethe-Universität Frankfurt, Frankfurt, Germany
- 64 Instituto de Ciencias Nucleares, Universidad Nacional Autónoma de México, Mexico City, Mexico
- 65 Instituto de Física, Universidade Federal do Rio Grande do Sul (UFRGS), Porto Alegre, Brazil
- 66 Instituto de Física, Universidad Nacional Autónoma de México, Mexico City, Mexico
- 67 iThemba LABS, National Research Foundation, Somerset West, South Africa
- 68 Jeonbuk National University, Jeonju, Republic of Korea
- 69 Johann-Wolfgang-Goethe Universität Frankfurt Institut für Informatik, Fachbereich Informatik und Mathematik, Frankfurt, Germany
- 70 Korea Institute of Science and Technology Information, Daejeon, Republic of Korea
- 71 KTO Karatay University, Konya, Turkey
- 72 Laboratoire de Physique des 2 Infinis, Irène Joliot-Curie, Orsay, France
- 73 Laboratoire de Physique Subatomique et de Cosmologie, Université Grenoble-Alpes, CNRS-IN2P3, Grenoble, France
- 74 Lawrence Berkeley National Laboratory, Berkeley, California, United States
- 75 Lund University Department of Physics, Division of Particle Physics, Lund, Sweden
- 76 Nagasaki Institute of Applied Science, Nagasaki, Japan
- 77 Nara Women's University (NWU), Nara, Japan
- 78 National and Kapodistrian University of Athens, School of Science, Department of Physics, Athens, Greece
- 79 National Centre for Nuclear Research, Warsaw, Poland
- 80 National Institute of Science Education and Research, Homi Bhabha National Institute, Jatni, India
- 81 National Nuclear Research Center, Baku, Azerbaijan
- 82 National Research and Innovation Agency - BRIN, Jakarta, Indonesia
- 83 Niels Bohr Institute, University of Copenhagen, Copenhagen, Denmark
- 84 Nikhef, National institute for subatomic physics, Amsterdam, Netherlands
- 85 Nuclear Physics Group, STFC Daresbury Laboratory, Daresbury, United Kingdom
- 86 Nuclear Physics Institute of the Czech Academy of Sciences, Husinec-Řež, Czech Republic
- 87 Oak Ridge National Laboratory, Oak Ridge, Tennessee, United States
- 88 Ohio State University, Columbus, Ohio, United States
- 89 Physics department, Faculty of science, University of Zagreb, Zagreb, Croatia
- 90 Physics Department, Panjab University, Chandigarh, India
- 91 Physics Department, University of Jammu, Jammu, India
- 92 Physics Department, University of Rajasthan, Jaipur, India
- 93 Physics Program and International Institute for Sustainability with Knotted Chiral Meta Matter (SKCM2), Hiroshima University, Hiroshima, Japan

- ⁹⁴ Physikalisches Institut, Eberhard-Karls-Universität Tübingen, Tübingen, Germany
⁹⁵ Physikalisches Institut, Ruprecht-Karls-Universität Heidelberg, Heidelberg, Germany
⁹⁶ Physik Department, Technische Universität München, Munich, Germany
⁹⁷ Politecnico di Bari and Sezione INFN, Bari, Italy
⁹⁸ Research Division and ExtreMe Matter Institute EMMI, GSI Helmholtzzentrum für Schwerionenforschung GmbH, Darmstadt, Germany
⁹⁹ Saha Institute of Nuclear Physics, Homi Bhabha National Institute, Kolkata, India
¹⁰⁰ School of Physics and Astronomy, University of Birmingham, Birmingham, United Kingdom
¹⁰¹ Sección Física, Departamento de Ciencias, Pontificia Universidad Católica del Perú, Lima, Peru
¹⁰² Stefan Meyer Institut für Subatomare Physik (SMI), Vienna, Austria
¹⁰³ SUBATECH, IMT Atlantique, Nantes Université, CNRS-IN2P3, Nantes, France
¹⁰⁴ Suranaree University of Technology, Nakhon Ratchasima, Thailand
¹⁰⁵ Technical University of Košice, Košice, Slovak Republic
¹⁰⁶ The Henryk Niewodniczanski Institute of Nuclear Physics, Polish Academy of Sciences, Cracow, Poland
¹⁰⁷ The University of Texas at Austin, Austin, Texas, United States
¹⁰⁸ Universidad Autónoma de Sinaloa, Culiacán, Mexico
¹⁰⁹ Universidade de São Paulo (USP), São Paulo, Brazil
¹¹⁰ Universidade Estadual de Campinas (UNICAMP), Campinas, Brazil
¹¹¹ Universidade Federal do ABC, Santo Andre, Brazil
¹¹² University of Cape Town, Cape Town, South Africa
¹¹³ University of Houston, Houston, Texas, United States
¹¹⁴ University of Jyväskylä, Jyväskylä, Finland
¹¹⁵ University of Kansas, Lawrence, Kansas, United States
¹¹⁶ University of Liverpool, Liverpool, United Kingdom
¹¹⁷ University of Science and Technology of China, Hefei, China
¹¹⁸ University of South-Eastern Norway, Kongsberg, Norway
¹¹⁹ University of Tennessee, Knoxville, Tennessee, United States
¹²⁰ University of the Witwatersrand, Johannesburg, South Africa
¹²¹ University of Tokyo, Tokyo, Japan
¹²² University of Tsukuba, Tsukuba, Japan
¹²³ University Politehnica of Bucharest, Bucharest, Romania
¹²⁴ Université Clermont Auvergne, CNRS/IN2P3, LPC, Clermont-Ferrand, France
¹²⁵ Université de Lyon, CNRS/IN2P3, Institut de Physique des 2 Infinis de Lyon, Lyon, France
¹²⁶ Université de Strasbourg, CNRS, IPHC UMR 7178, F-67000 Strasbourg, France, Strasbourg, France
¹²⁷ Université Paris-Saclay Centre d'Etudes de Saclay (CEA), IRFU, Département de Physique Nucléaire (DPhN), Saclay, France
¹²⁸ Università degli Studi di Foggia, Foggia, Italy
¹²⁹ Università del Piemonte Orientale, Vercelli, Italy
¹³⁰ Università di Brescia, Brescia, Italy
¹³¹ Variable Energy Cyclotron Centre, Homi Bhabha National Institute, Kolkata, India
¹³² Warsaw University of Technology, Warsaw, Poland
¹³³ Wayne State University, Detroit, Michigan, United States
¹³⁴ Westfälische Wilhelms-Universität Münster, Institut für Kernphysik, Münster, Germany
¹³⁵ Wigner Research Centre for Physics, Budapest, Hungary
¹³⁶ Yale University, New Haven, Connecticut, United States
¹³⁷ Yonsei University, Seoul, Republic of Korea
¹³⁸ Zentrum für Technologie und Transfer (ZTT), Worms, Germany
¹³⁹ Affiliated with an institute covered by a cooperation agreement with CERN
¹⁴⁰ Affiliated with an international laboratory covered by a cooperation agreement with CERN.